

Adaptive time-stepping exponential integrators for cubic-quintic complex Ginzburg-Landau equations

X. Ding^{a,*}, S. H. Kang^b

^aCenter for Nonlinear Science, School of Physics, Georgia Institute of Technology, Atlanta, GA 30332-0430, USA

^bSchool of Mathematics, Georgia Institute of Technology, Atlanta, GA 30332-0430, USA

Abstract

This paper is a survey on exponential integrators to solve cubic-quintic complex Ginzburg-Landau equations and related stiff problems. In particular, we are interested in accurate computation near the explosive soliton solutions where two different time scales exist. We explore time adaptive variations of three types of exponential integrators: integrating factor (IF) methods, exponential Runge-Kutta (ERK) methods and split-step (SS) methods, and their embedded versions for computation and comparison. We present the details, derive formulas for completeness, and consider seven different adaptive time-stepping integrating schemes to solve the cubic-quintic complex Ginzburg-Landau equation. Moreover, we propose using a comoving frame to resolve fast phase rotation for better performance. We present thorough comparisons and experiments in the one- and two-dimensional cubic-quintic complex Ginzburg-Landau equations.

Keywords: adaptive time-stepping, cubic-quintic complex Ginzburg-Landau, comoving frame, integrating factor methods, exponential Runge-Kutta methods, split-step methods

1. Introduction

The complex Ginzburg-Landau equation [1, 2] is one of the most frequently studied nonlinear equations in physics and applied mathematics community. In the context of pattern formation [1], it can be derived as a general amplitude equation near bifurcation point and has applications in various fields of physics ranging from nonlinear optics [3] to superconductivity [4]. Due to symmetry constraints, complex Ginzburg-Landau equation can only have odd-order nonlinear terms. Its cubic form is frequently used to study turbulence and intermittent traveling waves. Recently, complex Ginzburg-Landau equation with an additional quintic term

$$A_t = \mu A + (D_r + iD_i)\Delta A + (\beta_r + i\beta_i)|A|^2 A + (\gamma_r + i\gamma_i)|A|^4 A \quad (1)$$

has attracted attention for its peculiar dissipative soliton solutions in one- and two-dimensional cases [3, 5–9]. Here, $A(x, t)$ or $A(x, y, t)$ is a complex field. For the one- or two-dimensional case, the Laplace operator $\Delta = \partial_{xx}$ or $\Delta = \partial_{xx} + \partial_{yy}$ respectively. Among all the discoveries, solitons which undergo intermittent explosions stand out. An explosive soliton moves like a particle for the most time, but occasionally its profile changes substantially, then quickly restores back to the pre-explosion profile. This novel phenomenon offers a new direction in the research of complex Ginzburg-Landau equation, and proposes a numerical challenge, i.e., how to efficiently integrate the two different movements which have quite different time scales? The purpose of this paper is to introduce several adaptive time-stepping schemes to integrate cubic-quintic complex Ginzburg-Landau equation in the parameter region that soliton solutions explode.

*Corresponding author

Email addresses: xding@gatech.edu (X. Ding), kang@math.gatech.edu (S. H. Kang)

Explosive solitons were first discovered in the study of nonlinear optics [3, 6] and later realized in mode-locked lasers [10]. We briefly mention the one-dimensional form used in nonlinear optics,

$$i\psi_z + \frac{D}{2}\psi_{tt} + |\psi|^2\psi + \nu|\psi|^4\psi = i\delta\psi + i\beta\psi_{tt} + i\epsilon|\psi|^2\psi + i\mu|\psi|^4\psi, \quad (2)$$

where $\psi(t, z)$ is the envelope of the optical field, z and t are the propagation distance and the retarded time respectively, D is the group velocity dispersion coefficient, β stands for spectral filtering, δ and ϵ are the linear and nonlinear gain coefficients respectively. μ and ν , if negative, are the saturation coefficients of nonlinear gain and nonlinear saturation index. The correspondence of the two sets of parameters in (1) and (2) can be derived easily [11]. Throughout this paper, we use equation form (1) and enforce periodic boundary condition $x \in [0, L]$ or $(x, y) \in [0, L_x] \times [0, L_y]$ for one- and two-dimensional cases respectively. Following [11–14], we set the parameters in (1) to

$$\mu = -0.1, \quad D_r = 0.125, \quad D_i = 0.5, \quad \beta_r = 1, \quad \beta_i = 0.8, \quad \gamma_r = -0.1, \quad \gamma_i = -0.6$$

in order to observe symmetric and asymmetric explosions. We set domain size $L = L_x = L_y = 50$ which is large enough to hold a single soliton in the domain.

Taking advantage of the periodic boundary condition, we use pseudo-spectral method [15] to transform (1) into a set of ODEs in the Fourier space, i.e.,

$$\dot{a}_k = [\mu + (D_r + iD_i)q_k^2]a_k + (\beta_r + i\beta_i)\mathcal{F}_k(|A|^2A) + (\gamma_r + i\gamma_i)\mathcal{F}_k(|A|^4A) \quad (3)$$

for the one-dimensional case, and

$$\dot{a}_{mn} = [\mu + (D_r + iD_i)(q_m^2 + q_n^2)]a_{mn} + (\beta_r + i\beta_i)\mathcal{F}_{mn}(|A|^2A) + (\gamma_r + i\gamma_i)\mathcal{F}_{mn}(|A|^4A) \quad (4)$$

for the two-dimensional case. Here, $q_k = 2\pi k/L$. a_k and a_{mn} are the k th Fourier mode of $A(x, t)$ and m th Fourier mode of $A(x, y, t)$ respectively. $\mathcal{F}_k(\cdot)$ and $\mathcal{F}_{mn}(\cdot)$ denote the k th and m th component of the one- and two-dimensional discrete Fourier transform respectively. The velocity fields of (3) and (4) are split into a linear part and a nonlinear part. The linear parts are stiff due to the quadratic structure. Consequently, popular single-step integrators such as Runge-Kutta methods tend to use an extremely small stepping size, and thus we explore exponential integrators. Moreover, due to the two different time scales associated with explosive soliton solutions, time-step adaption is needed for exponential integrators.

In this paper, we investigate the performance of three different types of adaptive time-stepping exponential integrators, for single-step exponential integrators. Our motivation is to tackle cubic-quintic complex Ginzburg-Landau equation, and to the best of our knowledge, this is the first work to apply these methods to the explosive soliton integration in cubic-quintic complex Ginzburg-Landau equations. The main contributions of this paper are as follows. First, we note that the *Runge-Kutta methods in the interaction picture* used in the quantum mechanics community are equivalent to the integrating factor (IF) methods that will be explained in sect. 2.1. We not only convert two popular integrating factor methods and four popular exponential Runge-Kutta methods to their time adaptive versions, but also consider one split-step method with symmetric coefficients. Second, we formulate an embedded lower-order method in a 4th-order exponential Runge-Kutta method in table 6 without an additional internal stage and are the first to study the embedded 5th-order exponential Runge-Kutta method which will be introduced in sect. 3. Third, we utilize invariant dynamical structures in the system to accelerate the integration process. We compute traveling waves in cubic-quintic complex Ginzburg-Landau equations and integrate the system in a comoving frame with respect to the traveling waves. This change of frame promotes the performance of exponential Runge-Kutta methods, which will be covered in sect. 6. Finally, we experiment and compare these methods, to numerically solve the explosive soliton integration in cubic-quintic complex Ginzburg-Landau equations effectively.

This paper is organized as follows. In sect. 2, we review three different types of exponential integrators: integrating factor (IF) methods, exponential Runge-Kutta (ERK) methods and split-step (SS) methods. In sect. 3, we discuss how to embed a lower-order scheme in an exponential integrator and introduce seven representative schemes. The strategy to update step size and the metrics to evaluate the performance of an integrator is discussed in sect. 4. Sect. 5 is devoted to the numerical experiments on the one-dimensional cubic-quintic complex Ginzburg-Landau equation. We

compare the performance of constant time-stepping schemes with that of adaptive time-stepping schemes. In sect. 6, we introduce the idea of a comoving frame and use it to alleviate the fast-phase rotation problem. The performance of exponential Runge-Kutta schemes is improved in the comoving frame. Sect. 7 is devoted to the discussion of the performance of adaptive time-stepping schemes in the two-dimensional cubic-quintic complex Ginzburg-Landau equation. We summarize our discoveries in sect. 8.

2. An overview of exponential integrators

Both equations (3) and (4) belong to the semilinear problem of type:

$$y'(t) = f(t, y) = \mathcal{L}y + \mathcal{N}(t, y). \quad (5)$$

Here, linear operator \mathcal{L} is stiff. To cope with the stiffness, exponential integrators integrate the linear part explicitly and approximate the nonlinear part by expansion series. There are basically three different types of single-step exponential integrators: integrating factor (IF) methods, exponential Runge-Kutta (ERK) methods, and split-step (SS) methods. Both IF and ERK are Runge-Kutta based methods. They fill out Butcher tables by exponential functions of \mathcal{L} and derive order conditions similar to ordinary Runge-Kutta methods. ERK methods are very popular in the applied mathematics community. See ref. [16] for a detailed survey of IF and ERK methods. SS methods split a single integration step into several substeps and integrate the system forward by considering only the linear and nonlinear effect interchangeably. SS methods are frequently used in physics community especially in the nonlinear optics field. In this section, we give an overview of IF, ERK and SS methods applied to solving semilinear problem (5).

2.1. IF methods

The IF method is also called Lawson method [17] which dates back to 1967. It alleviates the stiffness of the linear part in (5) by a change of variables, i.e., $z(t) = e^{-t\mathcal{L}}y(t)$, resulting in a nonlinear system of the new variable

$$z'(t) = e^{-t\mathcal{L}}\mathcal{N}(t, e^{t\mathcal{L}}z). \quad (6)$$

Here, $e^{-t\mathcal{L}}$ is the integrating factor. This transformation effectively stabilizes this system because the linear part is integrated explicitly and the new Jacobian

$$e^{-t\mathcal{L}} \cdot \frac{\partial \mathcal{N}(t, y)}{\partial y} \Big|_{y=e^{t\mathcal{L}}z} \cdot e^{t\mathcal{L}}$$

has the same spectrum as that of the original Jacobian $\partial \mathcal{N}(t, y)/\partial y$, which is assumed to be nonstiff. After this transformation, popular time-stepping schemes are free to be applied to solve the new system (6). Lawson [17] first used the 4th-order Runge-Kutta method to integrate the new system, after which, various single-/multiple-step schemes have been implemented for (6). See [18] for all these variants.

On the other hand, in the quantum mechanics community, IF got another name *Runge-Kutta methods in the interaction picture* and was first used to integrate the time-dependent Gross-Pitaevskii equation by Caradoc-Davies [19]. The transformation used in this scenario is $z(t) = e^{-(t-t')\mathcal{L}}y(t)$ with $t' = t_n + \frac{1}{2}h_n$ during period t_n to t_{n+1} . Here $h_n = t_{n+1} - t_n$. The name originates from the exponential transformation from the Schrödinger picture to the interaction picture and implies that the latter will simplify the calculation. Later, this transformation is applied to the (generalized) nonlinear Schrödinger equation by Johan Hult [20]. He also compared it with SS methods, and thus made it well recognized in the optical fibers community.

In this paper, we apply Runge-Kutta schemes to equation (6). Substituting (6) into a general s -stage explicit Runge-Kutta scheme

$$Y_i = y_n + h \sum_{j=1}^{i-1} a_{ij}f(t_n + c_jh, Y_j), \quad y_{n+1} = y_n + h \sum_{i=1}^s b_i f(t_n + c_ih, Y_i),$$

we obtain

$$Y_i = e^{hc_i\mathcal{L}}y_n + h \sum_{j=1}^{i-1} a_{ij}e^{h\alpha_{ij}\mathcal{L}}\mathcal{N}(t_n + c_jh, Y_j), \quad y_{n+1} = e^{h\mathcal{L}}y_n + h \sum_{i=1}^s b_i e^{h\beta_i\mathcal{L}}\mathcal{N}(t_n + c_ih, Y_i), \quad (7)$$

where $\beta_i = 1 - c_i$ and $\alpha_{ij} = c_i - c_j$. The local error is estimated by embedding a lower-order Runge-Kutta method in (7). In Sect. 3, we consider two representative adaptive time-stepping IF schemes.

We note that IF methods have the disadvantage of producing large error coefficients when the linear term \mathcal{L} has a large norm, and they do not preserve fixed points of the original system (5). (For an improvement to generalize IF methods, see [21].) Even with these two drawbacks, IF methods have a benefit of an easy implementation, and we consider them for cubic-quintic complex Ginzburg-Landau equations.

2.2. ERK methods

ERK methods were originally used in computational electrodynamics [22], and have been widely used in other fields of physics [23–25]. In the early literatures, ERK methods are often referred to as *exponential time differencing* methods. As with IF methods, an ERK method also integrates the linear part explicitly. However, instead of a change of variables, an ERK method resorts to the exact integration of (5) from t_n to t_{n+1} by the variation-of-constants formula

$$y(t_{n+1}) = e^{h\mathcal{L}}y(t_n) + h \int_0^1 e^{(1-\theta)h\mathcal{L}}\mathcal{N}(t_n + \theta h, y(t_n + \theta h)) d\theta. \quad (8)$$

Here, $h = t_{n+1} - t_n$ is the time step. In order to approximate the integral part above, a polynomial interpolation at s non-confluent quadrature nodes c_1, \dots, c_s is applied to $\mathcal{N}(t_n + \theta h, y(t_n + \theta h))$, that is,

$$\mathcal{N}(t_n + \theta h, y(t_n + \theta h)) = \sum_{i=1}^s \prod_{j \neq i} \frac{\theta - c_j}{c_i - c_j} \mathcal{N}(t_n + c_i h, y(t_n + c_i h)).$$

So we get

$$y(t_{n+1}) = e^{h\mathcal{L}}y(t_n) + h \sum_{i=1}^s b_i(h\mathcal{L})\mathcal{N}(t_n + c_i h, y(t_n + c_i h)), \quad b_i(h\mathcal{L}) = \int_0^1 e^{(1-\theta)h\mathcal{L}} \prod_{j \neq i} \frac{\theta - c_j}{c_i - c_j} d\theta. \quad (9)$$

Similar to an explicit Runge-Kutta method, $y(t_n + c_i h)$ can be approximated as a combination of $y(t_n + c_j h)$ for $j < i$, we then obtain ERK method

$$Y_i = e^{hc_i\mathcal{L}}y_n + h \sum_{j=1}^{i-1} a_{ij}(h\mathcal{L})\mathcal{N}(t_n + c_j h, Y_j), \quad y_{n+1} = e^{h\mathcal{L}}y_n + h \sum_{i=1}^s b_i(h\mathcal{L})\mathcal{N}(t_n + c_i h, Y_i). \quad (10)$$

This scheme can be obtained by replacing $a_{ij}e^{h\alpha_{ij}\mathcal{L}}$ and $b_i e^{h\beta_i\mathcal{L}}$ in (7) with functions $a_{ij}(h\mathcal{L})$ and $b_i(h\mathcal{L})$. Here, coefficient functions $a_{ij}(h\mathcal{L})$ and $b_i(h\mathcal{L})$ are chosen as linear combinations of functions $\varphi_j(h\mathcal{L})$,

$$\varphi_j(z) = \int_0^1 e^{(1-\theta)z} \frac{\theta^{j-1}}{(j-1)!} d\theta, \quad j \geq 1.$$

It can be easily verified that $b_i(h\mathcal{L})$ in (9) is indeed a linear combination of $\varphi_j(h\mathcal{L})$. Furthermore, to gain a quick intuition for the choice of $\varphi_j(h\mathcal{L})$, we expand the nonlinear part in (8) with respect to θ and get

$$y(t_{n+1}) = e^{h\mathcal{L}}y(t_n) + h \sum_{r=0}^{\infty} h^r \mathcal{N}^{(r)} \int_0^1 \frac{e^{(1-\theta)h\mathcal{L}} \theta^r}{r!} d\theta = e^{h\mathcal{L}}y(t_n) + h \sum_{r=0}^{\infty} h^r \mathcal{N}^{(r)} \varphi_{r+1}(h\mathcal{L}).$$

Here, $\mathcal{N}^{(r)}$ is the r th derivative of \mathcal{N} with respect to θ . If we define $\varphi_0(z) = e^z$, then $\varphi_j(z)$ has a recursion relation

$$\varphi_{j+1}(z) = \frac{\varphi_j(z) - 1/j!}{z}, \quad \varphi_j(0) = \lim_{z \rightarrow 0} \varphi_j(z) = \frac{1}{j!}, \quad j \geq 0. \quad (11)$$

The first few $\varphi_j(z)$ are

$$\varphi_1(z) = \frac{e^z - 1}{z}, \quad \varphi_2(z) = \frac{e^z - z - 1}{z^2}, \quad \varphi_3(z) = \frac{e^z - z^2/2 - z - 1}{z^3}. \quad (12)$$

Similar to ordinary Runge-Kutta schemes, to achieve a certain order of accuracy, coefficient functions $a_{ij}(h\mathcal{L})$ and $b_i(h\mathcal{L})$ in (10) should satisfy a set of conditions. Order conditions of ERK methods were developed in two directions: *nonstiff order conditions* and *stiff order conditions*. Friedli [26] first derived nonstiff order conditions up to order 5 by matching Taylor series expansions of the exact and the numerical solutions. Later, the conditions were extended to an arbitrary order by using *B-series* [27]. The basic procedure is to expand $a_{ij}(h\mathcal{L})$ and $b_i(h\mathcal{L})$ in power series of $h\mathcal{L}$ and truncate them to a certain order; then order conditions are obtained by matching the coefficients of h with the same order on both sides of (10). This process is problematic when $h\mathcal{L}$ has a large norm, which means nonstiff order conditions are blind to the stiffness of the problem. To account for the stiffness, stiff order conditions up to order 4 were first given in [28]. Luan and Ostermann [29] gave the 5th-order conditions by a perturbation analysis after reformulating the scheme as a perturbation of the exponential Euler method. Later, they generalized the stiff order conditions to an arbitrary order by using *exponential B-series* [30]. Another benefit of stiff order conditions is that they preserve the equilibria of the original system [28]. Stiff order conditions up to order 3 are listed in table 1, in which $\psi_{j,i}(h\mathcal{L}) = \sum_{k=2}^{i-1} a_{ik}(h\mathcal{L})c_k^{j-1}/(j-1)! - c_i^j \varphi_j(c_i h\mathcal{L})$.

Table 1: Stiff order conditions for ERK up to order 3. Here, $z = h\mathcal{L}$. J denotes an arbitrary square matrix in the 5th stiff order condition. For the table up to order 5, see [29].

Order	Index	Stiff order condition
1	1	$\sum_{i=1}^s b_i(z) = \varphi_1(z)$
2	2	$\sum_{i=2}^s b_i(z)c_i = \varphi_2(z)$
	3	$\sum_{j=1}^{i-1} a_{ij}(z) = c_i \varphi_1(c_i z), \quad i = 2, \dots, s$
3	4	$\sum_{i=2}^s b_i(z) \frac{c_i^2}{2!} = \varphi_3(z)$
	5	$\sum_{i=2}^s b_i(z) J \psi_{2,i}(z) = 0$

Given a scheme satisfying nonstiff order conditions, order reduction is observed [28] if the corresponding stiff order conditions are not satisfied. This does not imply that stiff order conditions are superior to the nonstiff order condition. Stiff order conditions are rather restrictive, and under favorable circumstances [28], schemes show a higher order of convergence than the order predicted by the general stiff order conditions. Moreover, for quite a few physically interesting PDEs [31], order reduction does not appear. The order behavior of an ERK method applied to a specific system is subtle. In this paper, we formulate adaptive time-stepping schemes whose stiff orders match their nonstiff orders.

2.3. SS methods

The main idea of SS methods is that if the velocity field of a physical system can be decomposed as a sum of several separable sub-processes, then integration in one step can be approximated by several consecutive substeps, in each of which only one sub-process takes effect. SS methods were first proposed in the 1950s by Bagrinovskii and Godunov [32]. It was also formulated by Strang [33] as an alternating-direction difference scheme. This scheme has been widely used in integrating Hamiltonian systems [34] and PDEs of semilinear type [31]. In (5), we split the velocity field into one linear and another nonlinear part. Then for an s -stage SS method, one step of integration is decomposed into $2s$ substeps as follows,

$$y_{n+1} = \phi_N(b_s h) \circ e^{a_s h \mathcal{L}} \circ \dots \circ \phi_N(b_1 h) \circ e^{a_1 h \mathcal{L}} \circ y_n \quad (13)$$

here, \circ is a composition operator. It means that the integration result of one sub-process is the input to the next sub-process. $\phi_{\mathcal{N}}$ denotes the integration operator induced only by the nonlinear part:

$$y'(t) = \mathcal{N}(t, y). \quad (14)$$

The local error in each step can be expressed in terms of commutator $[\mathcal{L}, \mathcal{N}] = \mathcal{L}\mathcal{N} - \mathcal{N}\mathcal{L}$. For the order condition theory of SS methods, see [34–37].

3. Embedded exponential integrators

For cubic-quintic complex Ginzburg-Landau equation, numerical schemes such as SS [8, 38], Adams-Bashforth [39], ERK [40], Runge-Kutta in interaction picture [20] and others have been used to integrate equations (3) or (4). However, none of them is efficient to integrate explosive soliton solutions which have different time scales. We prefer the integrator to dynamically change step sizes based on the estimated local integration error. Whalen, Brio and Moloney [41] incorporated time-step adaption into several IF and ERK schemes by embedding lower-order schemes in them. W. Auzinger and his coworkers [36, 42, 43] made time-step adaption possible in an SS method by embedding a lower- or same-order method.

In this section, we introduce seven representative embedded schemes. IF4(3) and IF5(4) are IF based methods, where the two numbers $a(b)$ indicate that the scheme is a th-order accurate with an embedded b th-order scheme. ERK4(3)2(2), ERK4(3)3(3), ERK4(3)4(3) and ERK5(4)5(4) are ERK based methods, where four numbers $a(b)c(d)$ represent the scheme has nonstiff order a and stiff order c , and the embedded scheme has nonstiff order b and stiff order d . For these six IF or ERK based schemes, we follow the first-same-as-last (FSAL) rule to embed lower-order schemes. Namely, the last stage is evaluated at the same point as the first stage of the next step. The last scheme is SS4(3) which is based on an SS method. This scheme is 4th-order accurate and there is an embedded 3rd-order scheme.

3.1. IF4(3) and IF5(4)

Formula (7) describes a general s -stage IF scheme. To estimate the local integration error in (7), we embed a lower-order scheme of form $\bar{y}_{n+1} = e^{h\mathcal{L}}y_n + h \sum_{i=1}^{s+1} \bar{b}_i e^{h\bar{b}_i\mathcal{L}} \mathcal{N}(t_n + c_i h, Y_i)$. Then the estimated local error becomes

$$E_{n+1} = \bar{y}_{n+1} - y_{n+1} = h \sum_{i=1}^{s+1} (\bar{b}_i - b_i) e^{h\bar{b}_i\mathcal{L}} \mathcal{N}(t_n + c_i h, Y_i).$$

Here, the embedded scheme has one more stage, that the summation is from 1 to $s + 1$. We consider two classical embedded Runge-Kutta schemes proposed by Dormand and Princes [44, 45]. One is 4th-order accurate and the other is 5th-order accurate. Each of them has a one-order-lower embedded scheme.

The corresponding IF schemes are IF4(3) in table 2 and IF5(4) in table 3. Notice in their Butcher tables, following FSAL rule, the last intermediate stage is the same as the stage of evaluating y_{n+1} . The expressions for their local error estimation are listed in table 8.

Table 2: Butcher table of IF4(3). Here, $z = h\mathcal{L}$.

0					
$\frac{1}{2}$	$\frac{1}{2}e^{z/2}$				
$\frac{1}{2}$	0	$\frac{1}{2}$			
1	0	0	$e^{z/2}$		
1	$\frac{1}{6}e^z$	$\frac{1}{3}e^{z/2}$	$\frac{1}{3}e^{z/2}$	$\frac{1}{6}$	
b_i	$\frac{1}{6}e^z$	$\frac{1}{3}e^{z/2}$	$\frac{1}{3}e^{z/2}$	$\frac{1}{6}$	
\bar{b}_i	$\frac{1}{6}e^z$	$\frac{1}{3}e^{z/2}$	$\frac{1}{3}e^{z/2}$	$\frac{1}{15}$	$\frac{1}{10}$

0							
$\frac{1}{5}$	$\frac{1}{5}e^{z/5}$						
$\frac{3}{10}$	$\frac{3}{40}e^{3z/10}$	$\frac{9}{40}e^{z/10}$					
$\frac{4}{5}$	$\frac{44}{45}e^{4z/5}$	$-\frac{56}{15}e^{3z/5}$	$\frac{32}{9}e^{z/2}$				
$\frac{8}{9}$	$\frac{19372}{6561}e^{8z/9}$	$-\frac{25360}{2187}e^{31z/45}$	$\frac{64448}{6561}e^{53z/90}$	$-\frac{212}{729}e^{4z/45}$			
1	$\frac{9017}{3168}e^z$	$-\frac{355}{33}e^{4z/5}$	$\frac{46732}{5247}e^{7z/10}$	$\frac{49}{176}e^{z/5}$	$-\frac{5103}{18656}e^{z/9}$		
1	$\frac{35}{384}e^z$	0	$\frac{500}{1113}e^{7z/10}$	$\frac{125}{192}e^{z/5}$	$-\frac{2187}{6784}e^{z/9}$	$\frac{11}{84}$	
b_i	$\frac{35}{384}e^z$	0	$\frac{500}{1113}e^{7z/10}$	$\frac{125}{192}e^{z/5}$	$-\frac{2187}{6784}e^{z/9}$	$\frac{11}{84}$	
\bar{b}_i	$\frac{5179}{57600}e^z$	0	$\frac{7571}{16695}e^{7z/10}$	$\frac{393}{640}e^{z/5}$	$-\frac{92097}{339200}e^{z/9}$	$\frac{187}{2100}$	$\frac{1}{40}$

Table 3: Butcher table of IF5(4). Here, $z = h\mathcal{L}$.

We give two representative embedded IF schemes, and one has the freedom to choose as many variations of these schemes. But, as mentioned in [41], caution should be exerted when ordinary embedded Runge-Kutta methods are imported into IF methods. If $\alpha_{ij} < 0$ in (7), then backward propagation in the intermediate stage $e^{\alpha_{ij}\mathcal{L}}$ is troublesome for some systems with unbounded negative linear parts. We note that IF4(3) was used by Balac and Mahé [46] in the interaction picture context.

3.2. ERK4(3)2(2), ERK4(3)3(3), ERK4(3)4(3) and ERK5(4)5(4)

We consider four different embedded ERK methods. The first one is ERK4(3)2(2) [47] invented by Cox and Matthews and was later improved by Kassam and Trefethen [31]. This scheme has nonstiff order 4 and stiff order 2, and the embedded scheme has nonstiff order 3 and stiff order 2. We embed the lower-order scheme as shown in table 4. Here, $\varphi_i = \varphi_i(h\mathcal{L})$ are the basis functions (11) and $\varphi_{i,j} = \varphi_i(c_j h\mathcal{L})$. As with embedded IF methods, ERK4(3)2(2) follows the FSAL rule.

Table 4: Butcher table of ERK4(3)2(2). Here, $\varphi_i = \varphi_i(h\mathcal{L})$, $\varphi_{i,j} = \varphi_i(c_j h\mathcal{L})$.

0					
$\frac{1}{2}$	$\frac{1}{2}\varphi_{1,2}$				
$\frac{1}{2}$	0	$\frac{1}{2}\varphi_{1,3}$			
1	$\frac{1}{2}\varphi_{1,3}(\varphi_{0,3} - 1)$	0	$\varphi_{1,3}$		
1	$\varphi_1 - 3\varphi_2 + 4\varphi_3$	$2\varphi_2 - 4\varphi_3$	$2\varphi_2 - 4\varphi_3$	$4\varphi_3 - \varphi_2$	
b_i	$\varphi_1 - 3\varphi_2 + 4\varphi_3$	$2\varphi_2 - 4\varphi_3$	$2\varphi_2 - 4\varphi_3$	$4\varphi_3 - \varphi_2$	0
\bar{b}_i	$\varphi_1 - 3\varphi_2 + 4\varphi_3$	$2\varphi_2 - 4\varphi_3$	$2\varphi_2 - 4\varphi_3$	0	$4\varphi_3 - \varphi_2$

The second one is ERK4(3)3(3) proposed by Krogstad [21] and is shown in table 5. Its Butcher table is slightly different from that of ERK4(3)2(2) but with better convergence and stability. This scheme has nonstiff order 4 and stiff order 3. Note, the stiff orders of both ERK4(3)2(2) and ERK4(3)3(3) do not match their nonstiff orders, but they are very popular and for moderate stiff systems, it is claimed [18] that it is hard to do much better than these two methods. Therefore, we consider these schemes for comparison. The embedded scheme in ERK4(3)3(3) is nonstiff 3rd order, stiff 3rd order.

The third scheme is ERK4(3)4(3) invented by Hochbruck and Ostermann [28]. Its Butcher table is shown in table 6. It is both nonstiff and stiff 4th-order accurate. We try to embed a lower-order scheme here, but the FSAL approach fails because the last node coefficient c_5 is $1/2$ not 1. Fortunately, we observe that $c_2 = c_3 = c_5$, so by setting

$$\bar{b}_2 = xb_5, \quad \bar{b}_3 = yb_5, \quad \bar{b}_5 = 0$$

with other b_i unchanged and choosing the appropriate x, y , we hope to embed a 3rd-order method. From table 1, we see that the 3rd stiff order condition is already satisfied. Furthermore, setting $x + y = 1$ ensures the 1st, 2nd and 4th stiff order conditions. Finally, setting $x = y = 1/2$ make the embedded method satisfy a weakened but sufficient [28]

Table 5: Butcher table of ERK4(3)3(3).

0					
$\frac{1}{2}$	$\frac{1}{2}\varphi_{1,2}$				
$\frac{1}{2}$	$\frac{1}{2}\varphi_{1,3} - \varphi_{2,3}$	$\varphi_{2,3}$			
1	$\varphi_{1,4} - 2\varphi_{2,4}$	0	$2\varphi_{2,4}$		
1	$\varphi_1 - 3\varphi_2 + 4\varphi_3$	$2\varphi_2 - 4\varphi_3$	$2\varphi_2 - 4\varphi_3$	$4\varphi_3 - \varphi_2$	
b_i	$\varphi_1 - 3\varphi_2 + 4\varphi_3$	$2\varphi_2 - 4\varphi_3$	$2\varphi_2 - 4\varphi_3$	$4\varphi_3 - \varphi_2$	0
\bar{b}_i	$\varphi_1 - 3\varphi_2 + 4\varphi_3$	$2\varphi_2 - 4\varphi_3$	$2\varphi_2 - 4\varphi_3$	0	$4\varphi_3 - \varphi_2$

5th stiff order condition. So the embedded scheme has stiff order 3. We verify that it is also nonstiff order 3. Note, compared with the FSAL approach, this embedding does not require one additional internal stage; thus saves one evaluation of the nonlinear function $\mathcal{N}(t, y)$.

Table 6: Butcher table of ERK4(3)4(3).

0					
$\frac{1}{2}$	$\frac{1}{2}\varphi_{1,2}$				
$\frac{1}{2}$	$\frac{1}{2}\varphi_{1,3} - \varphi_{2,3}$	$\varphi_{2,3}$			
1	$\varphi_{1,4} - 2\varphi_{2,4}$	$\varphi_{2,4}$	$\varphi_{2,4}$		
$\frac{1}{2}$	$\frac{1}{2}\varphi_{1,5} - 2a_{5,2} - a_{5,4}$	$a_{5,2}$	$a_{5,2}$	$\frac{1}{4}\varphi_{2,5} - a_{5,2}$	
b_i	$\varphi_1 - 3\varphi_2 + 4\varphi_3$	0	0	$-\varphi_2 + 4\varphi_3$	$4\varphi_2 - 8\varphi_3$
\bar{b}_i	$\varphi_1 - 3\varphi_2 + 4\varphi_3$	$2\varphi_2 - 4\varphi_3$	$2\varphi_2 - 4\varphi_3$	$-\varphi_2 + 4\varphi_3$	0

$$a_{5,2} = \frac{1}{2}\varphi_{2,5} - \varphi_{3,4} + \frac{1}{4}\varphi_{2,4} - \frac{1}{2}\varphi_{3,5}$$

The last scheme we consider is ERK5(4)4(4) formulated by Luan and Ostermann [48] shown in table 7. It is both nonstiff and stiff 5th-order accurate. Following the FSAL rule, we embed a nonstiff and stiff 4th-order scheme. Note, the general nonstiff order conditions are given in [27] by bi-colored trees, but conditions only up to order 4 are listed explicitly. For verification convenience, we derive the 5th-order conditions in Appendix A.

The Butcher table of an ERK method consists of matrix functions of $h\mathcal{L}$, so at first glance, the adaptive time-stepping strategy seems not efficient due to the cost associated with refilling the Butcher table every time we change time step h . However, for cubic-quintic complex Ginzburg-Landau equations, the linear part \mathcal{L} is diagonal, thus evaluation of $\varphi_j(h\mathcal{L})$ becomes an arithmetic calculation, which has linear complexity. Even for systems with non-diagonal linear parts, techniques such as Krylov-subspace methods can be deployed to accelerate matrix function evaluation. For more details, see [16].

There is another implementation issue associated with ERK methods. Direct evaluation of $\varphi_j(z)$ in (12) suffers from loss of accuracy when z is small. It is believed that the contour integral method proposed by Kassam and Trefethen [31] can resolve this problem effectively. For our implementation, we take this approach to calculate $\varphi_j(z)$.

3.3. SS4(3)

We introduce one representative embedded SS scheme in this section. A lower-order scheme can be embedded in (13) by using a different set of coefficients a_i and b_i . Not like IF or ERK methods, adaptive time-stepping SS methods do not require recalculation of any run-time coefficients, so time-step adaption can be implemented with nearly no additional cost. Recently, Auzinger and his coworkers [36, 42, 43] proposed and optimized over 30 different embedded SS schemes with real or complex coefficients a_i and b_i . They invented four different methods to estimate the local integration error, among which, they find that the palindromic-pair schemes tend to have minimal local integration error. See [36] for the details. Therefore, we focus on the palindromic-pair scheme,

$$(a_1, b_1, \dots, a_s, b_s) = (b_s, a_s, \dots, b_1, a_1), \quad (15)$$

Table 7: Butcher table of ERK5(4)5(4).

0									
$\frac{1}{2}$	$\frac{1}{2}\varphi_{1,2}$								
$\frac{1}{2}$	$\frac{1}{2}\varphi_{1,3} - \frac{1}{2}\varphi_{2,3}$	$\frac{1}{2}\varphi_{2,3}$							
$\frac{1}{4}$	$\frac{1}{4}\varphi_{1,4} - \frac{1}{8}\varphi_{2,4}$	0	$\frac{1}{8}\varphi_{2,4}$						
$\frac{1}{2}$	$\frac{1}{2}\varphi_{1,5} - \frac{3}{2}\varphi_{2,5} + 2\varphi_{3,5}$	0	$-\frac{1}{2}\varphi_{2,5} + 2\varphi_{3,5}$	$2\varphi_{2,5} - 4\varphi_{3,5}$					
$\frac{1}{5}$	$\frac{1}{5}\varphi_{1,6} - \frac{2}{25}\varphi_{2,6} - \frac{1}{2}a_{64}$	0	0	$a_{6,4}$	$\frac{2}{25}\varphi_{2,6} - \frac{1}{2}a_{6,4}$				
$\frac{2}{3}$	$\frac{2}{3}\varphi_{1,7} + \frac{125}{162}a_{64} - a_{75} - a_{76}$	0	0	$-\frac{125}{162}a_{64}$	a_{75}	a_{76}			
1	$\varphi_{1,8} - a_{85} - a_{86} - a_{87}$	0	0	0	a_{85}	a_{86}	a_{87}		
1	$\varphi_1 - b_6 - b_7 - b_8$	0	0	0	0	b_6	b_7	b_8	
b_i	$\varphi_1 - b_6 - b_7 - b_8$	0	0	0	0	b_6	b_7	b_8	0
\bar{b}_i	$\varphi_1 - b_6 - b_7 - b_8$	0	0	0	0	b_6	b_7	0	b_8

$$\begin{aligned}
a_{64} &= \frac{8}{25}\varphi_{2,6} - \frac{32}{125}\varphi_{3,6}, & a_{75} &= \frac{125}{1944}a_{64} - \frac{16}{27}\varphi_{2,7} + \frac{320}{81}\varphi_{3,7}, & a_{76} &= \frac{3125}{3888}a_{64} + \frac{100}{27}\varphi_{2,7} - \frac{800}{81}\varphi_{3,7}, \\
\phi &= \frac{5}{32}a_{64} - \frac{1}{28}\varphi_{2,6} + \frac{36}{175}\varphi_{2,7} - \frac{48}{25}\varphi_{3,7} + \frac{6}{175}\varphi_{4,6} + \frac{192}{35}\varphi_{4,7} + 6\varphi_{4,8}, & a_{85} &= \frac{208}{3}\varphi_{3,8} - \frac{16}{3}\varphi_{2,8} - 40\phi, \\
a_{86} &= -\frac{250}{3}\varphi_{3,8} + \frac{250}{21}\varphi_{2,8} + \frac{250}{7}\phi, & a_{87} &= -27\varphi_{3,8} + \frac{27}{14}\varphi_{2,8} + \frac{135}{7}\phi, & b_6 &= \frac{125}{14}\varphi_2 - \frac{625}{14}\varphi_3 + \frac{1125}{14}\varphi_4, \\
b_7 &= -\frac{27}{14}\varphi_2 + \frac{162}{7}\varphi_3 - \frac{405}{7}\varphi_4, & b_8 &= \frac{1}{2}\varphi_2 - \frac{13}{2}\varphi_3 + \frac{45}{2}\varphi_4
\end{aligned}$$

$$y_1 = \phi_N(b_s h) \circ e^{a_s h \mathcal{L}} \circ \dots \circ \phi_N(b_1 h) \circ e^{a_1 h \mathcal{L}} \circ y(t_n), \quad (16)$$

$$y_2 = e^{b_s h \mathcal{L}} \circ \phi_N(a_s h) \circ \dots \circ e^{b_1 h \mathcal{L}} \circ \phi_N(a_1 h) \circ y(t_n), \quad (17)$$

$$y_{n+1} = \frac{1}{2}(y_1 + y_2), \quad \bar{y}_{n+1} = \frac{1}{2}(y_1 - y_2).$$

The name comes from equation (15) which says that coefficients b_i are totally determined by a_i , i.e., $b_i = a_{s+1-i}$. States y_1 and y_2 mirror each other by switching roles of linear and nonlinear operators. They approximate $y(t_{n+1})$ with the same order of accuracy and their leading terms of the local error have the same magnitude but opposite signs, so y_{n+1} is the local extrapolation of y_1 and y_2 with one more order of accuracy. \bar{y}_{n+1} serves as an error estimator.

In this paper, we focus on SS4(3) a 3-stage palindromic-pair scheme with real coefficients. It is 4th-order accurate with an embedded 3rd-order scheme. Auzinger called it PP3/4A in [43]. The coefficients of SS4(3) are

$$(a_1, a_2, a_3) = (0.268330095781759925, -0.187991618799159782, 0.919661523017399857).$$

In (13), the linear part is integrated explicitly, and we need to solve (14) s times during each single step. For some systems such as the cubic complex Ginzburg-Landau equation and the nonlinear Schrödinger equation, (14) can be solved explicitly [49]. For the cubic-quintic complex Ginzburg-Landau equation, such explicit formula does not exist, thus we turn to numerical schemes to solve (14). For our implementation, we use the 4th-order Runge-Kutta scheme to solve (14) s times. There are many evaluations of the nonlinear function $\mathcal{N}(t, y)$ in a single step in (16) and (17), and we restrict ourselves to only considering SS4(3) in this paper.

4. Time-step adaption and performance metrics

Each adaptive time-stepping scheme mentioned in sect. 3 consist of a higher-order scheme and an embedded lower-order scheme. Though the local error is estimated for the lower-order scheme, inspired by the local extrapolation strategy, we take the higher-order scheme to integrate the system forward. The estimated local error may not reflect

the true local error of the higher-order scheme, but this is reasonable in order to get a higher-order integrator. Let rtol be the relative tolerance for the local error, then the attempted new step size is

$$h_{\text{attempt}} = s \cdot h, \quad s = v \left(\frac{\text{rtol} \cdot \|y_{n+1}\|_{\infty}}{\|E_{n+1}\|_{\infty}} \right)^{1/p}.$$

Here, E_{n+1} is the estimated local error for y_{n+1} . See expressions of E_{n+1} for all seven schemes in table 8. p is the order of the local error of the embedded scheme. v is a safe factor and is set to 0.9. Updating step size for each single step is not efficient because of the frequent recalculation of $h\mathcal{L}$ and other dependent coefficients. Also, to avoid step size oscillation, we update step size only when $s < 1$ or when the difference between h_{attempt} and h is large enough. So we adopt the *lazy adaption* strategy as in [41]:

$$\mu = \begin{cases} 0.4 & s < 0.4 \\ s & 0.4 \leq s < 0.85 \\ 0.85 & 0.85 \leq s < 1 \\ 1 & 1 \leq s < 1.25 \\ s & 1.25 \leq s < 4 \\ 4 & s \geq 4 \end{cases}$$

The rule for updating step size is then $h_{\text{new}} = \mu h$.

In order to compare the performance of different schemes, the following metrics are used.

- **Nn**: Number of evaluations of nonlinear function $\mathcal{N}(t, y)$ during the whole integration process. For complex systems, evaluations of $\mathcal{N}(t, y)$ take the majority part of the total integration time, thus we use **Nn** as one of the main metrics to compare different methods. **nn** denotes the number of evaluations of $\mathcal{N}(t, y)$ in a single step. Values of **nn** of seven different schemes are listed in table 8. Note that, in SS4(3), we use the 4th-order Runge-Kutta scheme to solve the nonlinear propagation equation (14). Thus its **nn** entry is 24.
- **Nab**: Number of calculations of coefficients a_{ij} or b_i during the whole integration process. **nab** denotes the number of distinct a_{ij} and b_i entries in a Butcher table. Elements in Butcher tables of IF and ERK methods are exponential matrix functions like $e^{h\mathcal{L}}$, which need to be recalculated whenever the step size is updated. Moreover, coefficients a_{ij} and b_i in ERK methods are evaluated by contour integrals, which need more time to calculate than those in IF methods. Thus we only consider evaluations of a_{ij} and b_i in ERK methods. Table 8 lists the **nab** values of seven different schemes. Note, **nab** of ERK4(3)2(2) is 4 not 6 thanks to an implementation strategy from [31].
- **Global relative accuracy**: By using a very small step size, one can obtain a solution relatively close to the “true” solution. The global relative accuracy of each adaptive time-stepping scheme is compared to this.
- **Wt**: wall-clock time used for the integration. It is measured on a desktop equipped with 6 Intel i7-4930K 3.40GHz cores and 32G memory.

5. Numerical experiments and comparisons

We explore the effectiveness of the seven adaptive time-stepping schemes in the one-dimensional cubic-quintic complex Ginzburg-Landau equation. Throughout this section, we use an asymmetric initial condition as an input

$$A(x, 0) = 2.5 \exp \left(-450 \left(\frac{x}{L} - \frac{1}{2} \right)^2 \right) + 0.2 \exp \left(-450 \left(\frac{x}{L} - \frac{2}{5} \right)^2 \right). \quad (18)$$

This initial condition has a Gaussian wave in the middle of the domain with a small perturbation on the left side. Note that (18) is real, but this is not required. Any other localized initial state is good to experiment as long as it evolves to the soliton attractor of this system.

Table 8: Characteristics of seven embedded scheme. ‘order’: the order of the local error of the embedded scheme. ‘nn’: the number of evaluations of $\mathcal{N}(t, y)$ in a single step. ‘nab’: the number of distinct a_{ij} and b_i entries in a Butcher table. ‘ E_{n+1} ’: the expression for the estimated local error.

scheme	order	nn	nab	E_{n+1}
IF4(3)	4	5	-	$\frac{1}{10}h [\mathcal{N}(t_n + h, Y_5) - \mathcal{N}(t_n + h, Y_4)]$
IF5(4)	5	7	-	$h \left\{ \frac{-71}{57600} \mathcal{N}(t_n, Y_1) + \frac{71}{16695} \mathcal{N}(t_n + \frac{3h}{10}, Y_3) \right.$ $\left. - \frac{71}{1920} \mathcal{N}(t_n + \frac{4h}{5}, Y_4) + \frac{17253}{339200} \mathcal{N}(t_n + \frac{8h}{9}, Y_4) \right.$ $\left. - \frac{22}{525} \mathcal{N}(t_n + h, Y_5) + \frac{1}{40} \mathcal{N}(t_n + h, Y_6) \right\}$
ERK4(3)2(2)	4	5	4	$b_4 h [\mathcal{N}(t_n + h, Y_5) - \mathcal{N}(t_n + h, Y_4)]$
ERK4(3)3(3)	4	5	8	$b_4 h [\mathcal{N}(t_n + h, Y_5) - \mathcal{N}(t_n + h, Y_4)]$
ERK4(3)4(3)	4	5	11	$b_5 h \left[\mathcal{N}(t_n + h, Y_5) - \frac{1}{2}(\mathcal{N}(t_n + h/2, Y_2) + \mathcal{N}(t_n + h/2, Y_3)) \right]$
ERK5(4)5(4)	5	9	23	$b_8 h [\mathcal{N}(t_n + h, Y_9) - \mathcal{N}(t_n + h, Y_8)]$
SS4(3)	4	24	-	$(y_1 - y_2)/2$

5.1. The performance of constant time-stepping schemes

First, for comparison purposes, we consider the constant time-stepping schemes to visualize the two time scales associated with soliton propagation in this system. As shown in figure 1(a), two asymmetric explosions appear during the integration time window $t \in [0, 20]$. The explosions take only small fractions of the total integration time, while, the soliton profile does not change for the rest. Figure 1(b) contrasts an exploding profile at $t = 7$ with a slow-moving profile at $t = 10$. There are several sharp holes in the center of the exploding profile which change locations and depths dramatically in a short time. These characteristics indicate that the fast-explosive part should be integrated with smaller step size to maintain a certain accuracy. Figure 1(c) displays the estimated local error during the integration process of panel (a). During the fast-explosive parts, the estimated local error bursts substantially, spanning 2 to 3 orders of magnitude. The fast-explosive parts are the main cause of the accuracy lose. Figure 1(d) shows the global relative accuracy of all these methods at $t = 20$. We use constant time-stepping ERK5(4)5(4) with $h = 20/2^{18} = 7.6 \times 10^{-5}$ as the “true” solution to compare with. The two slashed black lines with slope 4 and 5 respectively justify the orders of all these seven schemes. We see that all the 4th-order schemes have almost the same performance. The performance of 5th-order schemes is superior to that of 4th-order schemes. Also, for a large step size, i.e., $h \simeq 10^{-2}$, the performance of IF5(4) is not as good as that of ERK5(4)5(4).

5.2. The performance of adaptive time-stepping schemes

We explore the adaptive time-stepping schemes which control the local error at each integration step. Figure 2(a)(b) show the spatiotemporal profiles of soliton evolution produced by ERK4(3)2(2) and SS4(3) respectively. The fast-explosive parts are stretched compared to figure 1(a). Figure 2(c) plots the step sizes used during the integration process. Step size is reduced when explosions happen and return to the normal level after explosions end. IF4(3), ERK4(3)2(2), ERK4(3)3(3) and ERK4(3)4(3) have almost the same adaption pattern, while SS4(3) behaves more aggressively in the slow-moving parts. The explosions in Figure 2(b) are more stretched than those in Figure 2(a). Moreover, note that in Figure 2(c) the two holes of SS4(3) are slightly shifted to the left side compared to other 4th-order schemes. This is due to SS4(3) using large step sizes during slow-moving parts. Since $\text{rto1} = 10^{-10}$ is fixed, 5th-order methods use larger step sizes, shown in Figure 2(c). Also, ERK5(4)5(4) is more aggressive than IF5(4).

Figure 3 shows the performance of all the seven schemes. Panel (a) shows that rto1 effectively controls the relative global error of all schemes. A smaller rto1 usually produces a more accurate result. However, such tendency saturates for $\text{rto1} < 10^{-11}$. SS4(3) has the largest relative global error. This is reasonable because SS4(3) uses larger step sizes during slow-moving parts as shown in figure 2(c). The integrator should spend more time on the fast-explosive parts, and with an appropriate rto1 we can achieve a required global accuracy. Panel (c) shows the number of evaluations of the nonlinear function Nn versus rto1 . The two 5th-order schemes IF5(4) and ERK5(4)5(4) have the least Nn because they use far fewer steps even though there are more evaluations of the nonlinear function in

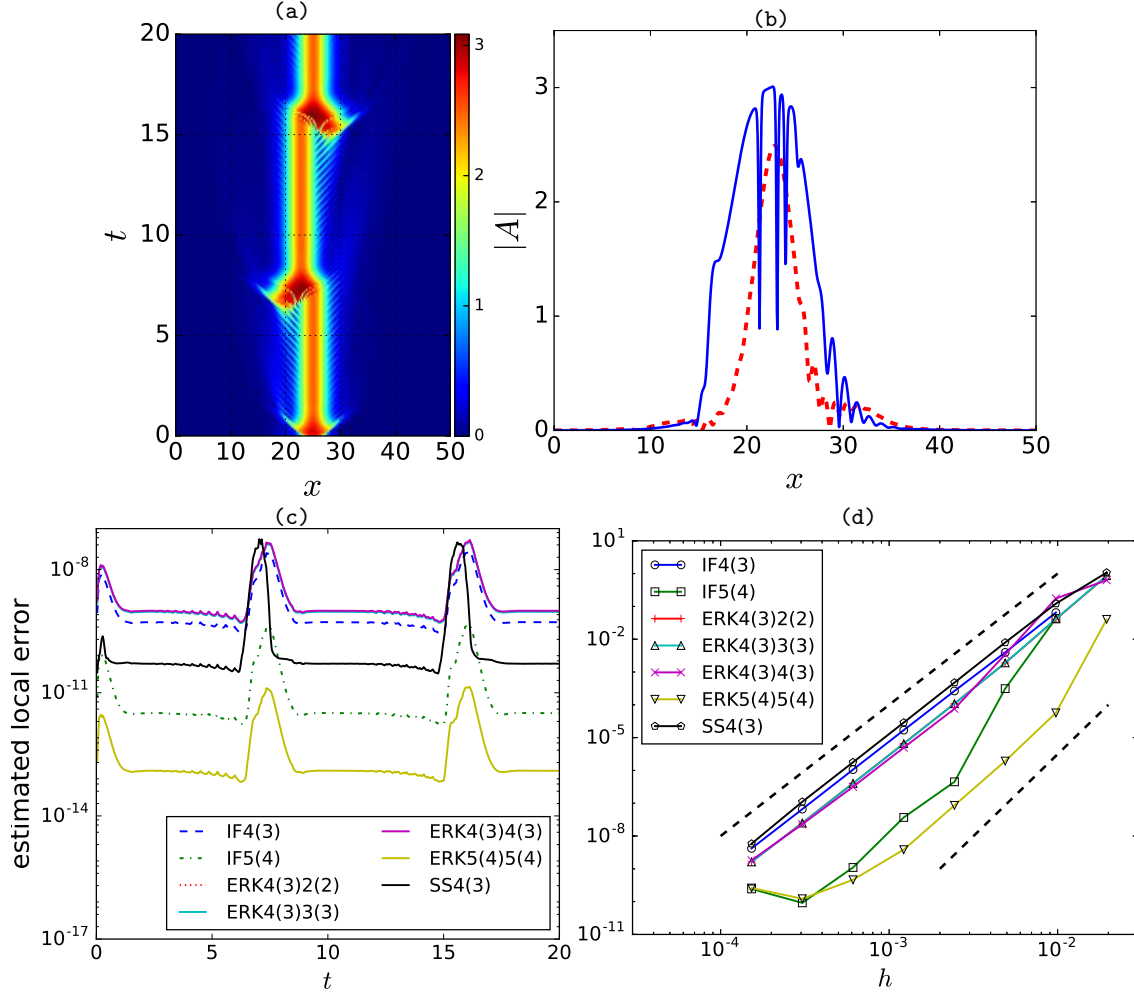


Figure 1: Evolution of initial condition (18) for $t \in [0, 20]$. (a) The spatiotemporal plot of field $|A(x, t)|$ by using $h = 2 \cdot 10^{-3}$. The color represents the magnitude of $|A(x, t)|$. (b) Profile of $|A(x, t)|$ at $t = 7$ (blue) and $t = 10$ (red). (c) Estimated local errors for constant step size $h = 20/2^{15} = 6.1 \times 10^{-4}$. (d) The global relative accuracy at the $t = 20$ for different choices of step sizes. The two dashed black lines have slope 4 and 5 respectively.

each step. Except for SS4(3), all other 4th-order schemes share a similar behavior of N_n . SS4(3) has a much larger N_n because there are 24 evaluations of $\mathcal{N}(t, y)$ in a single step for SS4(3). Panel (e) plots the wall time elapsed in seconds versus rtol . IF4(3), IF5(4) and SS4(3) have the same tendency as in panel (c). However, the relation saturates for ERK methods for a large rtol , which is most significant for ERK5(4)5(4). The reason is that, for IF4(3), IF5(4) and SS4(3), the integration time is mainly consumed by the calls to $\mathcal{N}(t, y)$. So, W_t is almost proportional to N_n .

While for ERK methods, refilling a Butcher table needs to evaluate contour integrals, and thus recalculation of a_{ij} and b_j constitutes a large part of the total time. As shown in panel (b), N_{ab} of ERK5(4)5(4) increases substantially when rtol gets beyond 10^{-11} , and for ERK4(3)2(2), ERK4(3)3(3) and ERK4(3)4(3), N_{ab} becomes slightly larger when rtol increases to 10^{-7} . The time used for refilling Butcher tables dominates W_t at large rtol for ERK methods. That is why wall time W_t saturates when rtol increases for ERK methods. This phenomenon raises another question: why does N_{ab} increase when rtol becomes large enough? N_{ab} is proportional to the number of times that a step size is rejected during the integration process. When rtol becomes larger, the step size will be larger and thus there is an increased possibility of step size oscillation in the integration process. Panel (d) shows that the number of rejections increases as rtol increases. The percentage of the time used to recalculate $h\mathcal{L}$ -dependent coefficients increases as well, as shown in panel (f). For ERK methods, refilling Butcher tables then becomes the most dominant factor of

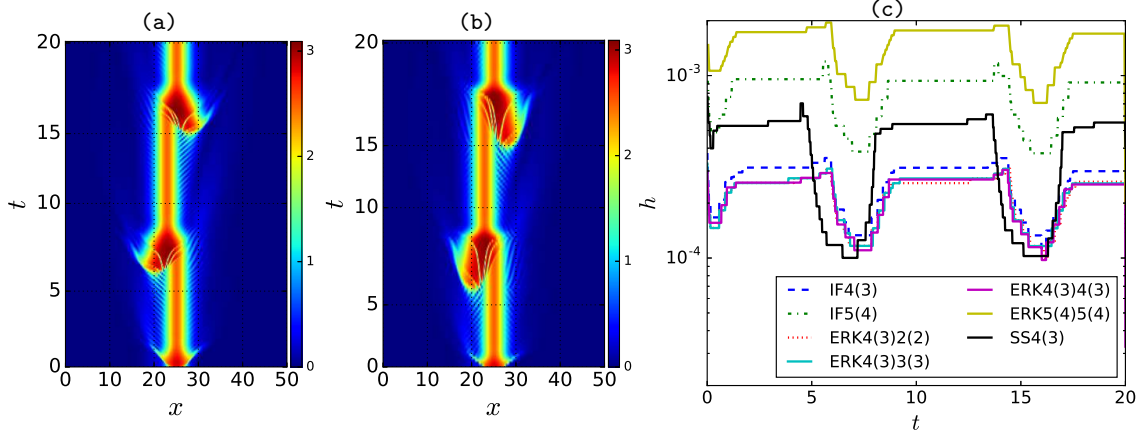


Figure 2: Evolution of initial condition (18) for $t \in [0, 20]$ using adaptive time-stepping schemes with $\text{rto1} = 10^{-10}$. (a)(b) Spatiotemporal plots of $|A(x, t)|$ produced by ERK4(3)2(2) and SS4(3) respectively. (c) Step sizes used during $t \in [0, 20]$.

performance. The time spent on refilling the Butcher table of ERK5(4)5(4) almost takes the whole computation time when rto1 reaches 10^{-9} as shown in panel (f).

In this section, we show that the adaptive time-stepping schemes effectively control the local error during the integration process. The two 5th-order schemes IF5(4) and ERK5(4)5(4) have the best performance. But the performance of ERK5(4)5(4) deteriorates when rto1 becomes too large.

6. Comoving-frame improvement for ERK methods

In sect. 5, we show that adaptive time-stepping schemes slow down the integration of fast-explosive parts, but the slow-moving parts still take the majority of computation time as we compare figure 2(a)(b) with figure 1(a). Also, figure 2(c) shows that there is a plateau for the step sizes used in the slow-moving parts. What stops us from using a larger step size is the *fast-phase rotation* of the complex field $A(x, t)$. Figure 4 shows the real part of the zeroth Fourier mode $\text{Re}(a_0)$ of $A(x, t)$ during the integration period in figure 1(a). The phase of a_0 rotates with a high frequency even though the profile $|A(x, t)|$ changes slowly in the slow-moving parts. Thus, if fast-phase rotation of complex field $A(x, t)$ can be handled effectively, one can further accelerate the slow-moving parts. We propose to use a comoving frame which has a similar rotating frequency as the original system. We show that the performance of ERK methods improves in this frame.

6.1. Dynamics in a comoving frame

To overcome the fast-phase rotation difficulty, we integrate the system in a comoving frame whose frequency is similar to the rotating frequency of $A(x, t)$. Let

$$A(x, t) = \tilde{A}(x, t)e^{i\Omega t}. \quad (19)$$

Here, Ω is the rotating frequency of this comoving frame. $A(x, t)$ and $\tilde{A}(x, t)$ is the state in the static and comoving frame respectively. Substituting (19) into the one-dimensional version of (1), we get

$$\tilde{A}_t = (\mu - i\Omega)\tilde{A} + (D_r + iD_i)\tilde{A}_{xx} + (\beta_r + i\beta_i)|\tilde{A}|^2\tilde{A} + (\gamma_r + i\gamma_i)|\tilde{A}|^4\tilde{A}. \quad (20)$$

By changing the real coefficient μ to the complex one $\mu - i\Omega$, we obtain the integrator in the comoving frame. Comoving frame introduces nearly no additional computational cost compared with the integrator in the static frame. The question now is how to pick the frequency of this comoving frame. One can simply measure the rotating frequency of $A(x, t)$ in the whole domain $x \in [0, L]$ for a certain slow-moving part and then obtain an average rotating rate. However, this approach is hard to automatize and other issues such as the wrap-around effect, i.e., aliasing, may

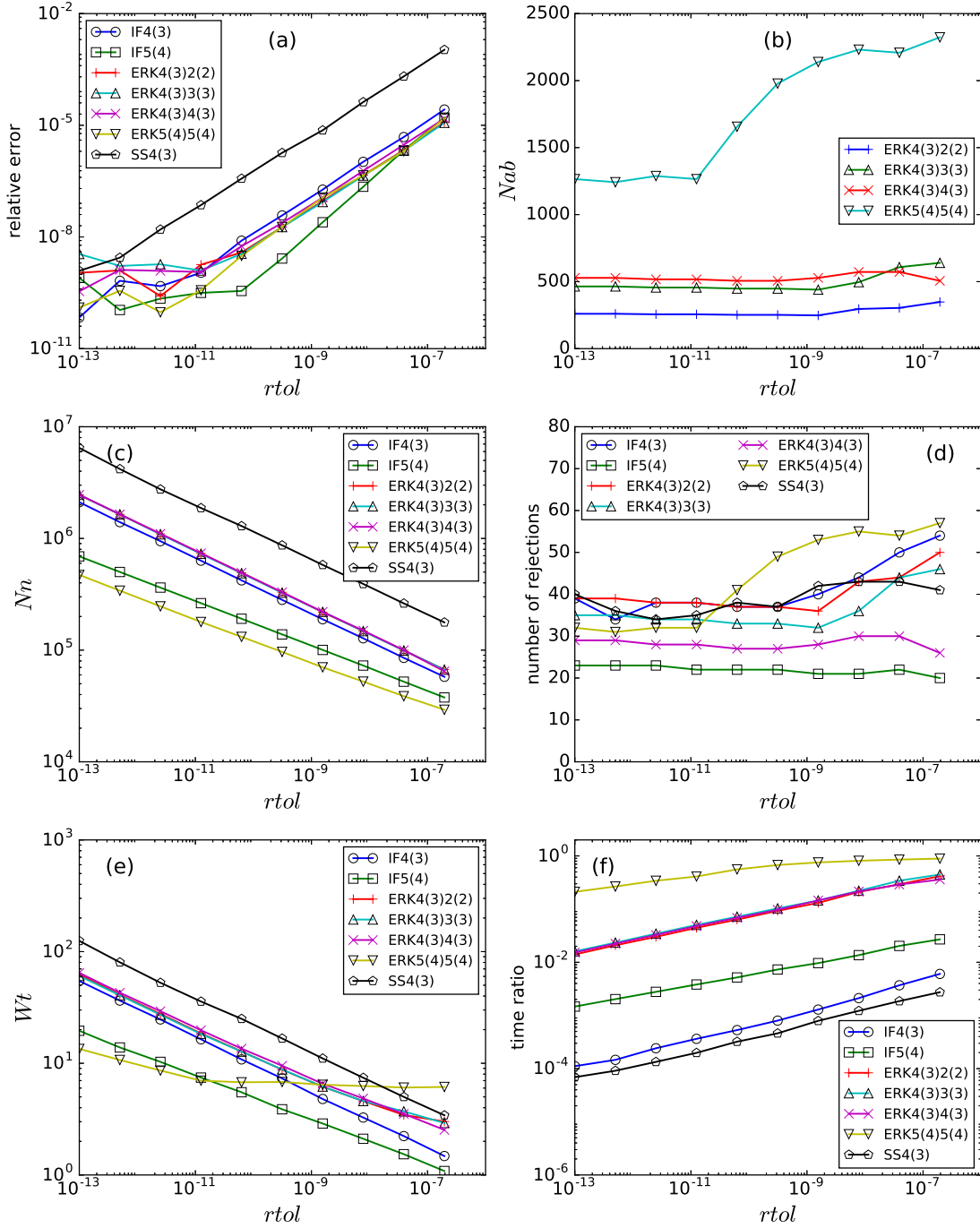


Figure 3: The performance of the seven adaptive time-stepping schemes.

complicate this process. In this paper, we take an approach which utilizes the underlining dynamically invariant structure of this exploding phenomenon.

Figure 1(a) illustrates that the basic structure of the dynamics is a slow-moving soliton which undergoes intermittent explosions. If we consider this soliton as a traveling wave, then an explosive part can be regarded as one

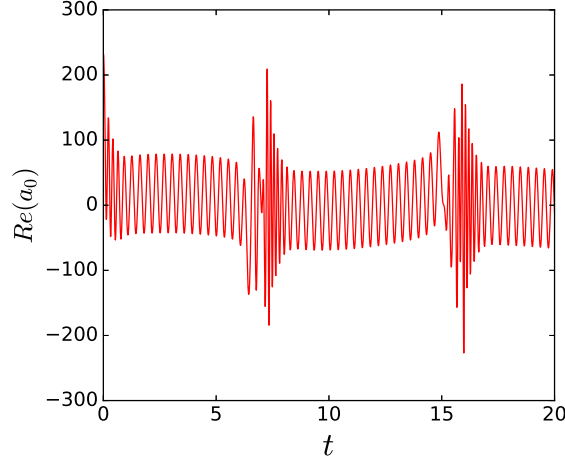


Figure 4: Real part of the zeroth Fourier mode of $A(x, t)$ versus time.

homoclinic orbit of this traveling wave. By a traveling wave, we mean an invariant solution of form

$$A(x, t) = A_0(x + ct)e^{i\omega t}. \quad (21)$$

Here, $A_0(x) = A(x, 0)$ is a localized field. Constants c and ω are spatial translation and phase velocity respectively. Definition (21) comes from the consideration of the two continuous symmetries of cubic-quintic complex Ginzburg-Landau equations. Equation (1) is invariant under spatial translation $A(x, t) \rightarrow A(x + \ell, t)$ and phase rotation $A(x, t) \rightarrow e^{i\phi} A(x, t)$. Soliton explosions result from the rapid growth of perturbations in the unstable directions of a traveling wave. The collapse of explosions is the result of dispersion effect. For more descriptive details, see [50]. Therefore, we set the frequency Ω of the comoving frame to the rotating frequency ω of this traveling wave, and integrate $\tilde{A}(x, t)$ instead of $A(x, t)$ for presumably better performance.

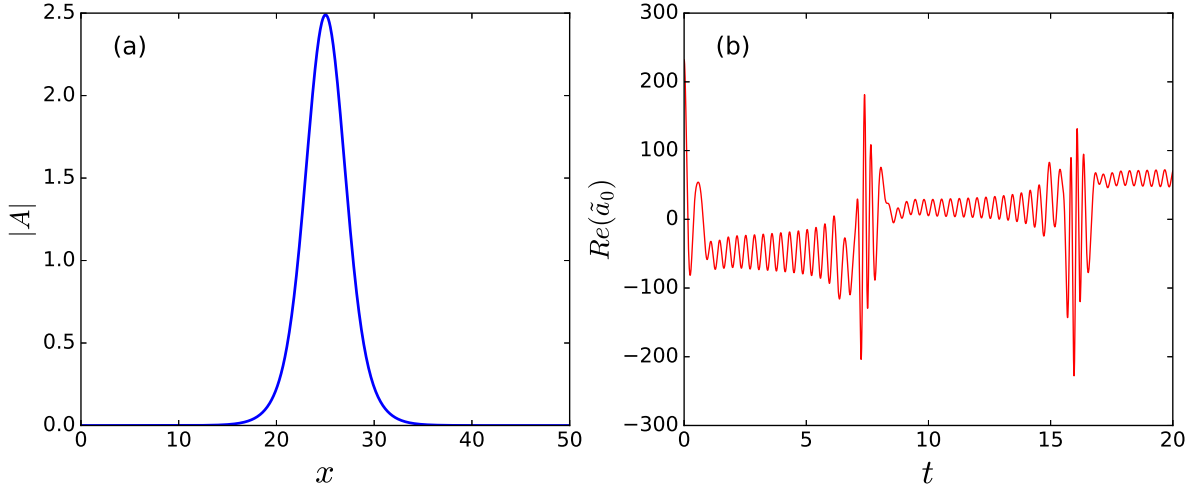


Figure 5: (a) Profile of the traveling wave. (b) Real part of the zeroth Fourier mode of $\tilde{A}(x, t)$ versus time.

To find the traveling wave, we consider the Fourier mode space, then equation (21) becomes

$$a_k(t) = \exp(i\omega t + ikq_c t) a_k(0), \quad k = 0, \pm 1, \pm 2, \dots$$

Here $q_c = 2\pi c/L$. Taking the time derivative on both sides, we get

$$\dot{a}_k(t) - ikq_c a_k - i\omega a_k = 0, \quad k = 0, \pm 1, \pm 2, \dots \quad (22)$$

Here velocity field \dot{a}_k is given in (3). Equation (22) defines an underdetermined system with respect to variables (a_k, c, ω) . Its roots are traveling waves. Given good initial guesses, Newton-based methods converge quadratically to the traveling wave solution. In practice, we use Levenberg-Marquardt algorithm [51, 52] for its larger convergence domain. The traveling wave obtained is shown in figure 5(a) with

$$c = 0, \quad \omega = 17.6675.$$

This traveling wave does not shift to the left or right side, but its phase rotates rapidly. By integrating in the comoving frame $\Omega = \omega$, we obtain $\text{Re}(\tilde{a}_0)$ shown in figure 5(b). \tilde{a}_0 is the zeroth Fourier mode of $\tilde{A}(x, t)$. Comparing it with figure 4, we see that the fast-phase rotation is effectively reduced at least for the slow-moving parts. Still, the explosion parts have fast-phase dynamics.

We emphasize that the traveling wave found for one specific set of parameters of the cubic-quintic complex Ginzburg-Landau equation can be used as an initial guess to find traveling waves in the parameter space. Finding an appropriate frequency of the comoving frame for different parameters can be easily automated.

6.2. Performance in the comoving frame

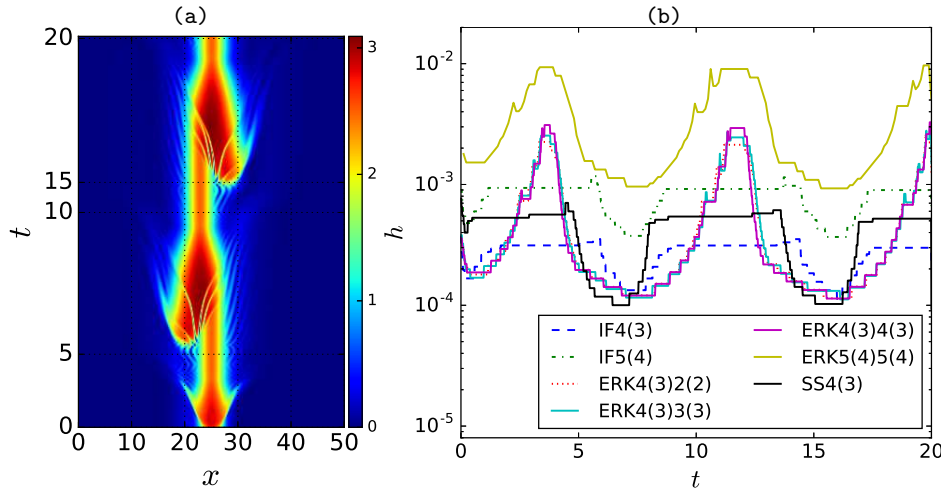


Figure 6: (a) Spatiotemporal plot of $|A(x, t)|$ produced by ERK4(3)2(2) in the comoving frame. (b) Step size h vs t when setting $\text{rtol} = 10^{-10}$ in the comoving frame.

Figure 6 (a) shows the integration result of ERK4(3)2(2) using the comoving frame. Comparing it with figure 2(a)(b) and figure 1(a), the slow moving part is sufficiently accelerated. Time steps used during integration process are shown in figure 6(b). There are several interesting observations comparing figure 6(b) with figure 2(c). First, for all seven methods, step sizes used during the fast-explosive parts are almost the same $h \simeq 10^{-4}$ in both static and comoving frame. This is reasonable because the comoving frame cannot reduce the rapid phase rotation during explosions.

Second, step sizes have increased substantially for ERK methods in the comoving frame for the slow-moving parts, while there is no change for IF4(3)4, IF5(4) and SS4(3) methods. The comoving frame only promotes the performance of ERK methods but does not for IF or SS methods. This intuitively contradictory result comes from the difference between the intermediate states among different methods. The comoving frame changes the linear part from \mathcal{L} to $\mathcal{L} - i\Omega$ in (20), and we discuss how this change affects the intermediate stages of IF, ERK and SS methods.

The intermediate state (7) of IF methods

$$Y_i = e^{hc_i\mathcal{L}}y_n + h \sum_{j=1}^{i-1} a_{ij}e^{h\alpha_{ij}\mathcal{L}}\mathcal{N}(t_n + c_jh, Y_j)$$

and the two Butcher tables, table 2 and table 3, show that coefficients $e^{hc_i\mathcal{L}}$ and $a_{ij}e^{h\alpha_{ij}\mathcal{L}}$ shift by $e^{-i\Omega c_ih}$ and $e^{-i\Omega\alpha_{ij}h}$ respectively. Assume Y_j , $j < i$, has shift $e^{-i\Omega c_jh}$, then $a_{ij}e^{h\alpha_{ij}\mathcal{L}}\mathcal{N}(t_n + c_jh, Y_j)$ has shift $e^{-i\Omega c_ih}$ because $\alpha_{ij} + c_j = c_i$. The intermediate state at $t_n + c_ih$ changes from Y_i to $Y_i e^{-i\Omega c_ih}$. Such a phase change only introduces a phase shift for the local error estimation in table 8. Therefore, IF methods are invariant under $\mathcal{L} \rightarrow \mathcal{L} - i\Omega$. For SS methods, both (16) and (17) have the same phase shift, so transformation $\mathcal{L} \rightarrow \mathcal{L} - i\Omega$ only introduces a phase rotation for the local error estimation and thus does not change the behavior of SS methods. However, for ERK methods (10), coefficients $a_{ij}(h\mathcal{L})$ and $b_i(h\mathcal{L})$ are functions of $\varphi_j(h\mathcal{L})$, which does not have an explicit phase rotation relation under transformation $\mathcal{L} \rightarrow \mathcal{L} - i\Omega$. So, intermediate state Y_i is not transformed to $Y e^{-i\Omega c_ih}$ as IF methods. The comoving frame modifies the local error estimation for ERK methods. For the slow-moving parts, the rapid phase rotation is effectively reduced using the comoving frame and intermediate states tend to have smaller differences in phase. Figure 6(b) illustrates how comoving frame accelerates the integration of the slow-moving parts.

We repeat the numerical experiments in figure 3 with a comoving frame. Figure 7 shows the corresponding statistics. The performance of IF4(3), IF5(4) and SS4(3) does not change in the comoving frame compared with that in the static frame. On the other hand, there are several differences for the ERK methods. Comparing figure 7(a) with figure 3(a), the global accuracy deteriorates in the comoving frame since larger step sizes are used for the slow-moving parts. Smaller `rtol` should be chosen in order to achieve the required global accuracy in the comoving frame for ERK methods. This is reasonable if one cares more about the percentage of time spent on the fast-explosive parts. Figure 7(c) shows that the number of evaluation of $\mathcal{N}(t, y)$ reduced significantly compared to the data in figure 3(c). The total integration time decreased as shown in figure 7(e). The number of times that a step size is rejected becomes 2 to 4 times larger in the comoving frame as shown in figure 7(d) compared to figure 3(d). For ERK5(4)5(4), the time for refilling the Butcher table takes the majority computation time even when `rtol` is as small as 10^{-13} , shown in figure 7(f). For a large `rtol`, ERK5(4)5(4) is not as efficient as other schemes, as indicated by figure 7(e).

In summary, the performance of ERK methods improves using a comoving frame. To have more time spent on the fast-explosive parts, one should use ERK4(3)2(2), ERK4(3)3(3), or ERK4(3)4(3), but not ERK5(4)5(4), since the last one spends too much time refilling its Butcher table.

7. Two-dimensional numerical experiments

We consider the two-dimensional cubic-quintic complex Ginzburg-Landau equation. We experiment and compare the different schemes, and explore the comoving frame in the two-dimensional setting. We discuss the similarities and difference compared to the one-dimensional case.

We use the following initial condition which represents a Gaussian wave at the center of the grid with a small perturbation in the southwest direction:

$$A(x, y, 0) = 2.5 \exp\left(-450\left(\frac{x}{L} - \frac{1}{2}\right)^2 - 450\left(\frac{y}{L} - \frac{1}{2}\right)^2\right) + 0.2 \exp\left(-450\left(\frac{x}{L} - \frac{2}{5}\right)^2 - 450\left(\frac{y}{L} - \frac{2}{5}\right)^2\right). \quad (23)$$

We integrate the system to $t = 20$, during which there are three explosions. The snapshots of one such explosion are shown in figure 8 (a)~(e). The profile of the soliton augments asymmetrically during this exploding process. Also, there are several sharp cracks in the center of the soliton in panel (c), which move and change from panel (c) to (d). All these fast-changing structures require a smaller step size to maintain a certain local integration accuracy compared to the step size needed before and after the explosion, i.e., panel (a) and (e) respectively.

Figure 9 shows the performance of the seven adaptive time-stepping schemes. Panel (a) shows the step sizes used during the integration. There are three dips in this figure, which represent that the integrators slow down during three exploding instances. IF5(4) and ERK5(4)5(4) use larger step sizes than those of 4th-order schemes. All 4th-order schemes use similar step sizes. Panel (b)~(f) show the performance measured by different metrics. The tendencies

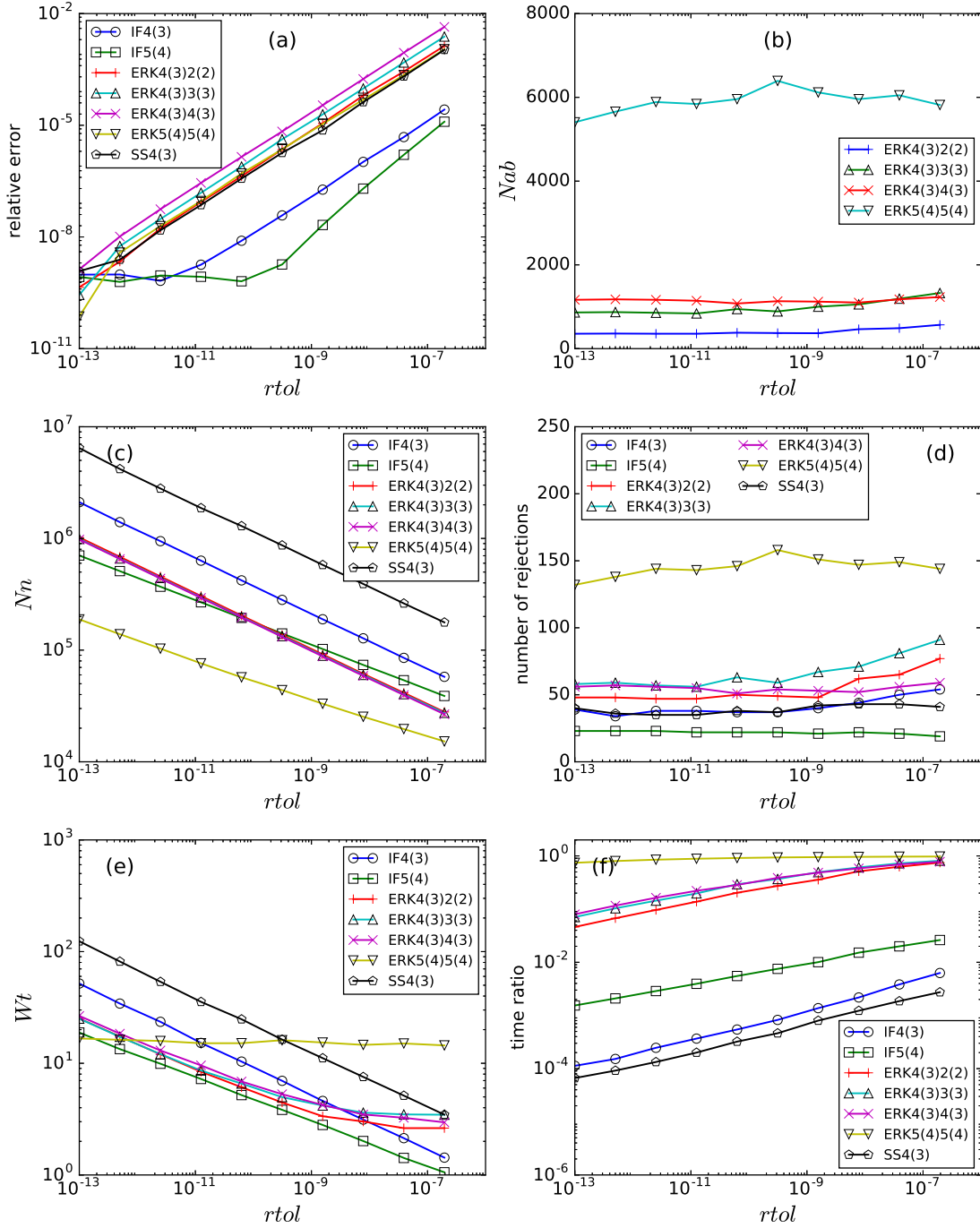


Figure 7: Same as figure 3 but in the comoving frame.

shown in panel (b)~(f) are very similar to those in figure 3. Among the four ERK methods, ERK5(4)5(4) has the largest number of times of calculating the elements of its Butcher table as shown in panel (b). Two facts account for this: First, there are 23 different elements in the Butcher table of ERK5(4)5(4), which are far more than other ERK methods. Second, as shown in panel (d), attempted trials of ERK5(4)5(4) are more likely to get rejected compare to

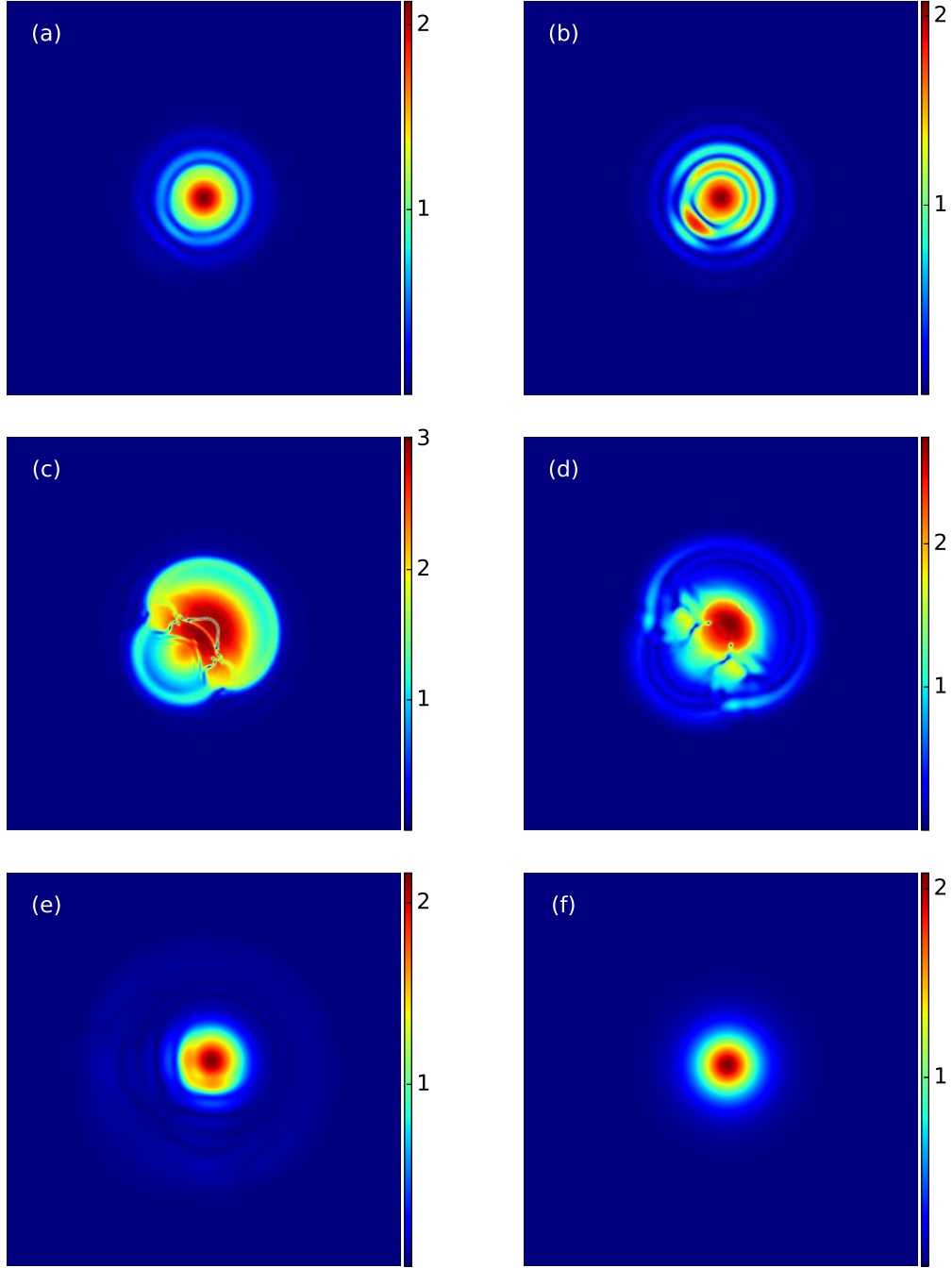


Figure 8: (a)~(e) Snapshots of one explosion in the two-dimensional cubic-quintic complex Ginzburg-Landau equation using initial condition (23). The system is integrated by ERK4(3)2(2). These five snapshots correspond to the state at $t = 3, 5, 8, 10, 12$ respectively. (f) The profile of an unstable traveling wave in this system. In all figures, the color represents the magnitude of $|A(x, y, t)|$.

other ERK methods. Panel (c) shows the number of evaluations of the nonlinear function. Similar to figure 3(c), the two 5th-order schemes have least evaluations of the nonlinear function. SS4(3) has the largest number of evaluations because it computes the nonlinear function 24 times in a single step. Panel (e) and (f) show the wall time of integration

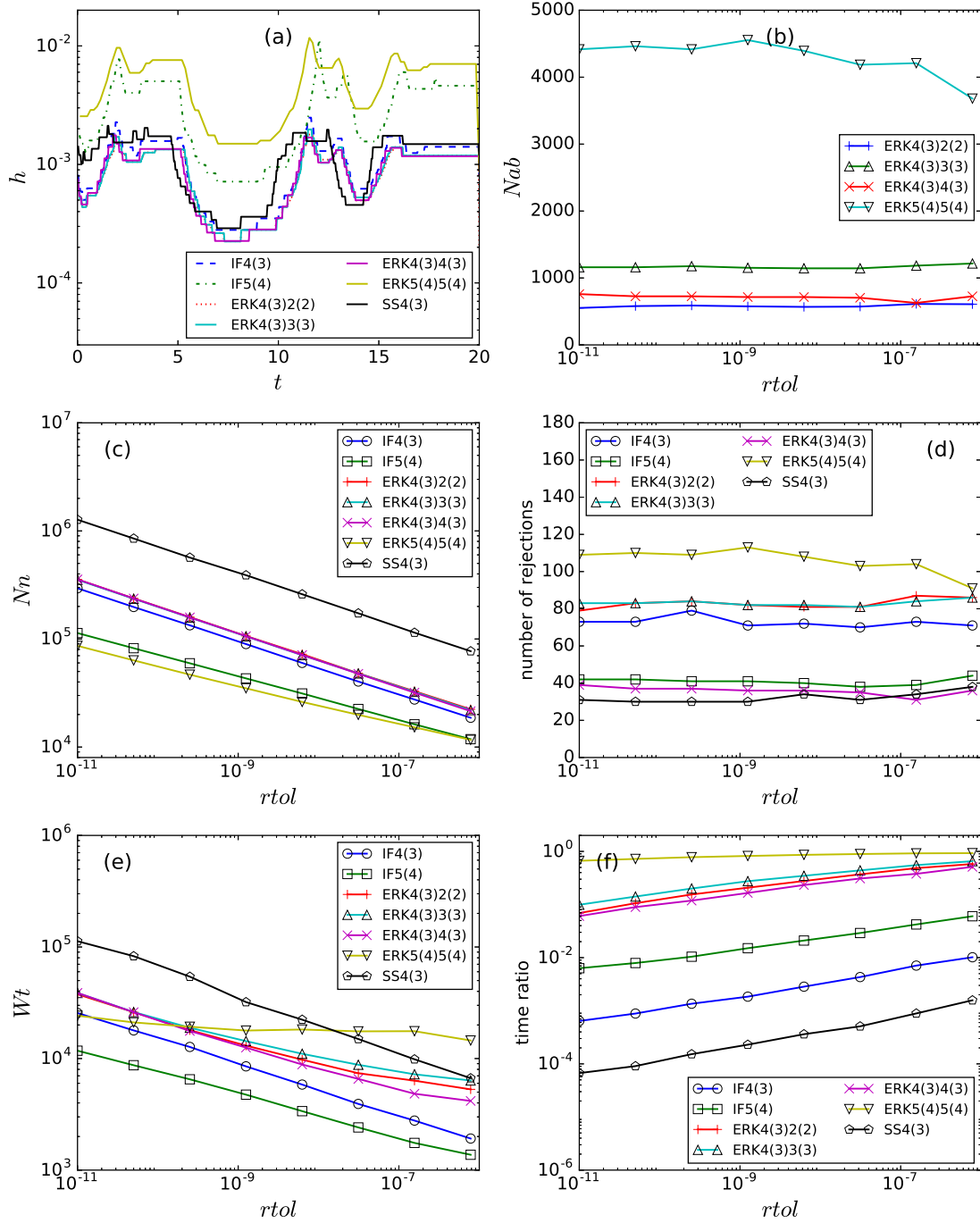


Figure 9: Performance of adaptive time-stepping schemes in the static frame for the two-dimensional cubic-quintic complex Ginzburg-Landau equation. (a) Step sizes used during the integration process when $rtol = 10^{-9}$. (b)–(f) Performance measured by different metrics when $rtol$ varies.

and the percentage of time spent on recalculating coefficients. The two-dimensional simulation is about 3- or 4-order more expensive than the one-dimensional simulation comparing panel (e) with figure 3(e). In the two-dimensional integration, ERK5(4)5(4) spends most of the time recalculating the coefficients. it is less efficient than the other

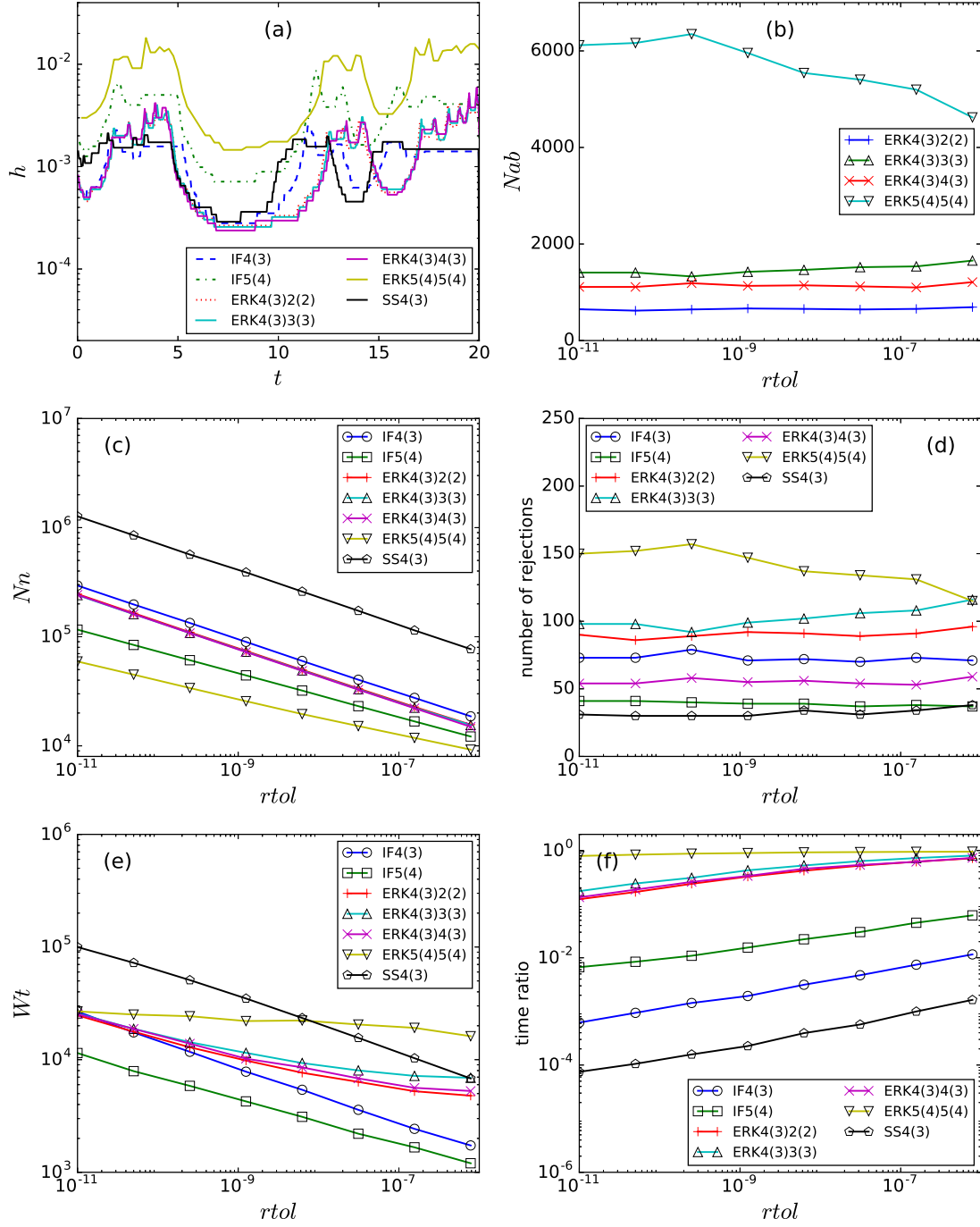


Figure 10: The same as figure 9 but in a comoving frame.

5th-order scheme IF5(4).

To compute the comoving frame, similar to the one-dimensional case, explosions in the two-dimensional cubic-quintic complex Ginzburg-Landau equation can be visualized as homoclinic orbits of an unstable traveling wave of

this system. A two-dimensional traveling wave has form

$$A(x, y, t) = A_0(x + c_x t, y + c_y t) e^{i\omega t},$$

with c_x , c_y , and ω respectively the translation velocity in the x , y direction, and the phase velocity. By a shooting method [53], we find a traveling wave with

$$c_x = 0, \quad c_y = 0, \quad \omega = 7.3982. \quad (24)$$

It has phase rotation but no spatial translation. Figure 8(f) shows the profile of this traveling wave. For the slow-moving parts, the system has a similar phase-rotation rate as this traveling wave. Therefore, similar to (19) and (20), we can define a comoving frame for the two-dimensional cubic-quintic complex Ginzburg-Landau equation.

Figure 10 displays the performance of the seven adaptive time-stepping schemes in the comoving frame. As in the case of one-dimensional, only the performance of ERK schemes is affected by the comoving frame. Comparing panel (a) in figure 9 and that in figure 10, the step sizes used during the slow-moving parts are about 2 to 3 times larger for ERK schemes in the comoving frame, which is manifest for the part after the third explosion. Also, for ERK schemes in panel (c), the number of times to evaluate the nonlinear function decreased insignificantly. However, the rejection rates increased for ERK schemes as shown in panel (d). As a consequence, the total integration time only decreased by a small amount as shown in panel (e). The improvement of performance in the comoving frame is not striking. The reason is that the phase velocity (24) is not large; thus the fast-phase rotation problem is not severe in the static frame. Therefore, to integrate the two-dimensional cubic-quintic complex Ginzburg-Landau equation with the parameters chosen in this paper, the best choice out of the seven schemes is IF5(4).

8. Conclusions

We explored seven adaptive time-stepping integrating schemes to one- and two-dimensional cubic-quintic complex Ginzburg-Landau equations. For explosive soliton solutions in these systems, two different time scales exist. The slow-moving part and the fast-explosive part should use different step sizes in order to integrate the system efficiently. By embedding lower order schemes in IF, ERK and SS methods, local integration error is controlled effectively. The step size is adapted to maintain a relative accuracy in each single integration step. We find that all these seven schemes use a smaller step size in the fast-explosive part than that used in the slow-moving part. Time-step adaption works well for integrating explosive soliton solutions in cubic-quintic complex Ginzburg-Landau equations. Moreover, to better handle the fast-phase rotation difficulty, we integrated the system in a comoving frame whose rotating frequency is similar to that of the soliton solution. We show that integration in the comoving frame can further accelerate the slow-moving parts for ERK methods.

In the one-dimensional case, the two 5th-order methods IF5(4) and ERK5(4)5(4) have the best performance. IF5(4) is easy to implement because it has a simple Butcher table structure. ERK5(4)5(4) can benefit from the comoving frame and remarkably slow down the fast-explosive parts. Since ERK5(4)5(4) spends a long time refilling its Butcher table when local error tolerance `rtol` becomes large, we prefer ERK5(4)5(4) when `rtol` is small but choose IF5(4) otherwise. In the two-dimensional case, we find that IF5(4) have the best performance. When the phase rotation is not very severe, a comoving frame may not improve the results much. Meanwhile, when one need to implement an adaptive time-stepping scheme quickly, then the 4th-order schemes are suitable. ERK4(3)2(2) may be the best choice among all 4th-order methods considered in this paper because of its simple Butcher table structure.

The main focus of this paper is to explore methods to experiment cubic-quintic complex Ginzburg-Landau equation. Nonetheless, these numerical schemes can be applied to other stiff (and non-stiff) systems that exhibit intermittent behaviors.

9. Acknowledgements

We are grateful to P. Cvitanović for providing insightful arguments about the phase rotation phenomenon in one-dimensional cubic-quintic complex Ginzburg-Landau equation. X.Ding is supported by a grant from G. Robinson, Jr.. S.H. Kang is supported by Simons Foundation grant 282311.

Appendix A.

Table A.9 displays the nonstiff 5th-order conditions. There are 37 equations. The first 26 come from adding a black or white node to the root node of the 4th-order bi-colored trees [27]. The remaining 11 equations are enumerated by counting the 2-fork type (8 equations), the 3-fork type (2 equations) and the 4-fork type (1 equation). For the general result to an arbitrary order, see ref. [27] (Theorem 2.1).

Table A.9: Nonstiff 5th-order conditions.

	Tree	condition		Tree	condition
1		$\sum \beta^{r,0} \alpha_r^{j,0} c_j^3 = \frac{1}{20}$	15		$\sum \beta^{r,0} \alpha_r^{j,0} \alpha_j^{k,1} c_k = \frac{1}{120}$
2		$\sum \beta^{r,1} c_r^3 = \frac{1}{20}$	16		$\sum \beta^{r,1} \alpha_r^{j,1} c_j = \frac{1}{120}$
3		$\sum \beta^{r,0} \alpha_r^{j,0} \alpha_j^{k,0} c_j c_k = \frac{1}{40}$	17		$\sum \beta^{r,0} \alpha_r^{j,0} \alpha_j^{k,2} = \frac{1}{120}$
4		$\sum \beta^{r,1} \alpha_r^{j,0} c_r c_j = \frac{1}{40}$	18		$\sum \beta^{r,1} \alpha_r^{j,2} = \frac{1}{120}$
5		$\sum \beta^{r,0} \alpha_r^{j,0} \alpha_j^{k,1} c_j = \frac{1}{40}$	19		$\sum \beta^{r,0} \alpha_r^{j,1} \alpha_j^{k,0} c_k = \frac{1}{120}$
6		$\sum \beta^{r,1} \alpha_r^{j,1} c_r = \frac{1}{40}$	20		$\sum \beta^{r,2} \alpha_r^{j,0} c_j = \frac{1}{120}$
7		$\sum \beta^{r,0} \alpha_r^{j,0} \alpha_j^{k,0} c_k^2 = \frac{1}{60}$	21		$\sum \beta^{r,0} \alpha_r^{j,1} \alpha_j^{k,1} = \frac{1}{120}$
8		$\sum \beta^{r,1} \alpha_r^{j,0} c_j^2 = \frac{1}{60}$	22		$\sum \beta^{r,2} \alpha_r^{j,1} = \frac{1}{120}$
9		$\sum \beta^{r,0} \alpha_r^{j,1} c_j^2 = \frac{1}{60}$	23		$\sum \beta^{r,0} \alpha_r^{j,2} c_j = \frac{1}{120}$
10		$\sum \beta^{r,2} c_r^2 = \frac{1}{60}$	24		$\sum \beta^{r,3} c_r = \frac{1}{120}$
11		$\sum \beta^{r,0} \alpha_r^{j,0} \alpha_j^{k,0} \alpha_k^{p,0} c_p = \frac{1}{120}$	25		$\sum \beta^{r,0} \alpha_r^{j,3} = \frac{1}{120}$
12		$\sum \beta^{r,1} \alpha_r^{j,0} \alpha_j^{k,0} c_k = \frac{1}{120}$	26		$\sum \beta^{r,4} = \frac{1}{120}$
13		$\sum \beta^{r,0} \alpha_r^{j,0} \alpha_j^{k,0} \alpha_k^{p,1} = \frac{1}{120}$			
14		$\sum \beta^{r,1} \alpha_r^{j,0} \alpha_j^{k,1} = \frac{1}{120}$			

	Tree	condition
27		$\sum \beta^{r,0} \alpha_r^{j,0} c_j^2 c_r = \frac{1}{15}$
28		$\sum \beta^{r,0} \alpha_r^{j,0} \alpha_j^{k,0} c_k c_r = \frac{1}{30}$
29		$\sum \beta^{r,0} \alpha_r^{j,0} \alpha_j^{k,1} c_r = \frac{1}{30}$
30		$\sum \beta^{r,0} \alpha_r^{j,0} c_j \alpha_r^{k,0} c_k = \frac{1}{20}$
31		$\sum \beta^{r,0} \alpha_r^{j,1} \alpha_r^{k,1} = \frac{1}{20}$
32		$\sum \beta^{r,0} \alpha_r^{j,0} c_j \alpha_r^{k,1} = \frac{1}{20}$
33		$\sum \beta^{r,0} c_r \alpha_r^{j,1} c_j = \frac{1}{30}$
34		$\sum \beta^{r,0} c_r \alpha_r^{j,2} = \frac{1}{30}$
35		$\sum \beta^{r,0} c_r^2 \alpha_r^{j,0} c_j = \frac{1}{10}$
36		$\sum \beta^{r,0} c_r^2 \alpha_r^{j,1} = \frac{1}{10}$
37		$\sum \beta^{r,0} c_r^4 = \frac{1}{5}$

References

References

- [1] M. C. Cross, P. C. Hohenberg, Pattern formation outside of equilibrium, Rev. Mod. Phys. 65 (1993) 851–1112. [doi:10.1103/RevModPhys.65.851](https://doi.org/10.1103/RevModPhys.65.851).
- [2] I. S. Aranson, L. Kramer, The world of complex Ginzburg-Landau equation, Rev. Mod. Phys. 74 (2002) 99–143. [doi:10.1103/RevModPhys.74.99](https://doi.org/10.1103/RevModPhys.74.99).
- [3] N. Akhmediev, J. M. Soto-Crespo, G. Town, Pulsating solitons, chaotic solitons, period doubling, and pulse coexistence in mode-locked lasers: Complex Ginzburg-Landau equation approach, Phys. Rev. E 63 (2001) 056602. [doi:10.1103/PhysRevE.63.056602](https://doi.org/10.1103/PhysRevE.63.056602).

- [4] V. L. Ginzburg, Nobel Lecture: On superconductivity and superfluidity (what i have and have not managed to do) as well as on the “physical minimum” at the beginning of the XXI century, *Rev. Mod. Phys.* 76 (2004) 981–998. doi:10.1103/RevModPhys.76.981.
- [5] W. Chang, A. Ankiewicz, N. Akhmediev, J. M. Soto-Crespo, Creeping solitons in dissipative systems and their bifurcations, *Phys. Rev. E* 76 (2007) 016607. doi:10.1103/PhysRevE.76.016607.
- [6] J. M. Soto-Crespo, N. Akhmediev, A. Ankiewicz, Pulsating, creeping, and erupting solitons in dissipative systems, *Phys. Rev. Lett.* 85 (2000) 2937–2940. doi:10.1103/PhysRevLett.85.2937.
- [7] J. M. Soto-Crespo, N. Akhmediev, K. S. Chiang, Simultaneous existence of a multiplicity of stable and unstable solitons in dissipative systems, *Phys. Lett. A* 291 (2001) 115–123. doi:10.1016/S0375-9601(01)00634-X.
- [8] C. Cartes, J. Cisternas, O. Descalzi, H. R. Brand, Model of a two-dimensional extended chaotic system: Evidence of diffusing dissipative solitons, *Phys. Rev. Lett.* 109 (2012) 178303. doi:10.1103/PhysRevLett.109.178303.
- [9] J. Cisternas, O. Descalzi, T. Albers, G. Radons, Anomalous diffusion of dissipative solitons in the cubic-quintic complex Ginzburg-Landau equation in two spatial dimensions, *Phys. Rev. Lett.* 116 (2016) 203901. doi:10.1103/PhysRevLett.116.203901.
- [10] S. T. Cundiff, J. M. Soto-Crespo, N. Akhmediev, Experimental evidence for soliton explosions, *Phys. Rev. Lett.* 88 (2002) 073903. doi:10.1103/PhysRevLett.88.073903.
- [11] O. Descalzi, H. R. Brand, Transition from modulated to exploding dissipative solitons: Hysteresis, dynamics, and analytic aspects, *Phys. Rev. E* 82 (2010) 026203. doi:10.1103/PhysRevE.82.026203.
- [12] J. Cisternas, O. Descalzi, C. Cartes, The transition to explosive solitons and the destruction of invariant tori, *Cent. Eur. J. Phys.* 10 (2012) 660–668. doi:10.2478/s11534-012-0023-1.
- [13] J. Cisternas, O. Descalzi, Intermittent explosions of dissipative solitons and noise-induced crisis, *Phys. Rev. E* 88 (2013) 022903. doi:10.1103/PhysRevE.88.022903.
- [14] N. Akhmediev, J. M. Soto-Crespo, Strongly asymmetric soliton explosions, *Phys. Rev. E* 70. doi:10.1103/PhysRevE.70.036613.
- [15] L. N. Trefethen, *Spectral Methods in MATLAB*, SIAM, Philadelphia, 2000. doi:10.1137/1.9780898719598.
- [16] M. Hochbruck, A. Ostermann, Exponential integrators, *Acta Numerica* 19 (2010) 209–286. doi:10.1017/S0962492910000048.
- [17] J. D. Lawson, Generalized Runge-Kutta processes for stable systems with large Lipschitz constants, *SIAM J. Numer. Anal.* 4 (1967) 372–380. doi:10.1137/0704033.
- [18] H. Montanelli, N. Bootland, *Solving stiff PDEs in 1D, 2D and 3D with exponential integrators* (2016). URL <http://arxiv.org/abs/1604.08900>
- [19] B. M. Caradoc-Davies, Vortex dynamics in Bose-Einstein condensates, Ph.D. thesis, Univ. Otago, Dunedin, New Zealand (2000).
- [20] J. Hult, A fourth-order Runge-Kutta in the interaction picture method for simulating supercontinuum generation in optical fibers, *J. Lightwave Technol.* 25 (2007) 3770–3775. doi:10.1109/JLT.2007.909373.
- [21] S. Krogstad, Generalized integrating factor methods for stiff PDEs, *J. Comput. Phys.* 203 (2005) 72–88. doi:10.1016/j.jcp.2004.08.006.
- [22] A. Taflov, S. C. Hagness, *Computational Electrodynamics: The Finite-difference Time-domain Method*, Artech House, 2005.
- [23] R. Holland, Finite-difference time-domain (FDTD) analysis of magnetic diffusion, *IEEE Trans. Electromagn. Compat.* 36 (1994) 32–39. doi:10.1109/15.265477.
- [24] P. G. Petropoulos, Analysis of exponential time-differencing for FDTD in lossy dielectrics, *IEEE Trans. Antennas Propag.* 45 (1997) 1054–1057. doi:10.1109/8.585755.
- [25] C. Schuster, A. Christ, W. Fichtner, Review of FDTD time-stepping schemes for efficient simulation of electric conductive media, *Microw. Opt. Technol. Lett.* 25 (2000) 16–21. doi:10.1002/(SICI)1098-2760(20000405)25:1<16::AID-MOP6>3.0.CO;2-O.
- [26] A. Friedli, Verallgemeinerte Runge-Kutta Verfahren zur Lösung steifer Differentialgleichungssysteme, in: R. Bulirsch, R. D. Grigorieff, J. Schröder (Eds.), *Numerical Treatment of Differential Equations: Proceedings of a Conference, Held at Oberwolfach, July 4–10, 1976*, Springer, Berlin, 1978, pp. 35–50. doi:10.1007/BFb0067462.
- [27] H. Berland, B. Owren, B. Skaflestad, B-series and order conditions for exponential integrators, *SIAM J. Numer. Anal.* 43 (2005) 1715–1727. doi:10.1137/040612683.
- [28] M. Hochbruck, A. Ostermann, Explicit exponential Runge-Kutta methods for semilinear parabolic problems, *SIAM J. Numer. Anal.* 43 (2005) 1069–1090. doi:10.1137/040611434.
- [29] V. T. Luan, A. Ostermann, Stiff order conditions for exponential Runge-Kutta methods of order five, in: G. H. Bock, P. X. Hoang, R. Rannacher, P. J. Schlöder (Eds.), *Modeling, Simulation and Optimization of Complex Processes - HPSC 2012: Proceedings of the Fifth International Conference on High Performance Scientific Computing, March 5-9, 2012, Hanoi, Vietnam*, Springer, Cham, 2014, pp. 133–143. doi:10.1007/978-3-319-09063-4_11.
- [30] V. T. Luan, A. Ostermann, Exponential B-series: The stiff case, *SIAM J. Numer. Anal.* 51 (2013) 3431–3445. doi:10.1137/130920204.
- [31] A.-K. Kassam, L. N. Trefethen, Fourth-order time-stepping for stiff PDEs, *SIAM J. Sci. Comput.* 26 (2005) 1214–1233. doi:10.1137/S1064827502410633.
- [32] K. A. Bagrinovskii, S. K. Godunov, Difference schemes for multi-dimensional problems, *Dokl. Acad. Nauk.* 115 (1957) 431–433.
- [33] G. Strang, On the construction and comparison of difference schemes, *SIAM J. Numer. Anal.* 5 (1968) 506–517. doi:10.1137/0705041.
- [34] H. Yoshida, Construction of higher order symplectic integrators, *Phys. Lett. A* 150 (1990) 262–268. doi:10.1016/0375-9601(90)90092-3.
- [35] W. Auzinger, W. Herfort, Local error structures and order conditions in terms of Lie elements for exponential splitting schemes, *Opuscula Math.* 34 (2014) 43–255. doi:10.7494/opmath.2014.34.2.243.
- [36] W. Auzinger, H. Hofstätter, D. Ketcheson, O. Koch, Practical splitting methods for the adaptive integration of nonlinear evolution equations. Part I: construction of optimized schemes and pairs of schemes, *BIT Numer. Math.* 57 (2016) 55–74. doi:10.1007/s10543-016-0626-9.
- [37] S. Blanes, F. Casas, A. Farrés, J. Laskar, J. Makazaga, A. Murua, New families of symplectic splitting methods for numerical integration in dynamical astronomy, *Appl. Numer. Math.* 68 (2013) 58–72. doi:10.1016/j.apnum.2013.01.003.
- [38] T. Mohammadi, A. Aissat, An accurate Fourier splitting scheme for solving the cubic-quintic complex Ginzburg-Landau equation, *Superlattices Microstruct.* 75 (2014) 424–434. doi:10.1016/j.spmi.2014.08.007.

- [39] F. Bérard, C.-J. Vandamme, S. C. Mancas, Two-dimensional structures in the quintic Ginzburg–Landau equation, *Nonlinear Dyn.* 81 (2015) 1413–1433. [doi:10.1007/s11071-015-2077-2](#).
- [40] A.-K. Kassam, L. N. Trefethen, Solving reaction-diffusion equations 10 times faster, Numerical Analysis Group Research Report 1192, Oxford University (2003).
- [41] P. Whalen, M. Brio, J. V. Moloney, Exponential time-differencing with embedded Runge-Kutta adaptive step control, *J. Comput. Phys.* 280 (2015) 579–601. [doi:10.1016/j.jcp.2014.09.038](#).
- [42] O. Koch, C. Neuhauser, M. Thalhammer, Embedded exponential operator splitting methods for the time integration of nonlinear evolution equations, *Appl. Numer. Math.* 63 (2013) 14–24. [doi:10.1016/j.apnum.2012.09.002](#).
- [43] W. Auzinger, O. Koch, M. Quell, Adaptive high-order splitting methods for systems of nonlinear evolution equations with periodic boundary conditions, *Numer. Algorithms* (2016) 1–23. [doi:10.1007/s11075-016-0206-8](#).
- [44] J. R. Dormand, P. J. Prince, New Runge-Kutta algorithms for numerical simulation in dynamical astronomy, *Celest. Mech.* 18 (1978) 223–232. [doi:10.1007/BF01230162](#).
- [45] J. R. Dormand, P. J. Prince, A family of embedded Runge-Kutta formulae, *J. Comput. Appl. Math.* 15 (1986) 203–211. [doi:10.1016/0771-050X\(80\)90013-3](#).
- [46] S. Balac, F. Mahé, Embedded Runge-Kutta scheme for step-size control in the interaction picture method, *Comput. Phys. Commun.* 184 (2013) 1211–1219. [doi:10.1016/j.cpc.2012.12.020](#).
- [47] S. M. Cox, P. C. Matthews, Exponential time differencing for stiff systems, *J. Comput. Phys.* 176 (2002) 430–455. [doi:10.1006/jcph.2002.6995](#).
- [48] V. T. Luan, A. Ostermann, Explicit exponential Runge–Kutta methods of high order for parabolic problems, *J. Comput. Appl. Math.* 256 (2014) 168–179. [doi:10.1016/j.cam.2013.07.027](#).
- [49] S. Wang, L. Zhang, An efficient split-step compact finite difference method for cubic–quintic complex Ginzburg–Landau equations, *Comput. Phys. Commun.* 184 (2013) 1511–1521. [doi:10.1016/j.cpc.2013.01.019](#).
- [50] X. Ding, P. Cvitanović, Exploding relative periodic orbits in cubic-quintic complex Ginzburg–Landau equation, in preparation (2017).
- [51] K. Levenberg, A method for the solution of certain non-linear problems in least squares, *Quart. Appl. Math.* 2 (1944) 164–168. [doi:10.1090/qam/10666](#).
- [52] D. M. Marquardt, An algorithm for least-squares estimation of nonlinear parameters, *J. Soc. Indust. Appl. Math.* 11 (1963) 431–441. [doi:10.1137/0111030](#).
- [53] G. J. Chandler, R. R. Kerswell, Invariant recurrent solutions embedded in a turbulent two-dimensional Kolmogorov flow, *J. Fluid Mech.* 722 (2013) 554–595. [doi:10.1017/jfm.2013.122](#).